

Laterally converging duct flows. Part 4. Temporal behaviour in the viscous layer

DONALD M. McELIGOT^{1,2,3,4†}, ROBERT S. BRODKEY⁵
AND HELMUT ECKELMANN^{6,7}

¹Aerospace and Mechanical Engineering Department, University of Arizona, Tucson, AZ 85721, USA

²Institut für Kernenergetik und Energiesysteme (IKE), Universität Stuttgart,
D-70569 Stuttgart, Deutschland

³Idaho National Laboratory (INL), Idaho Falls, ID 83415-3885, USA

⁴Stokes Research Institute, University of Limerick, Limerick, Ireland

⁵Chemical and Biomolecular Engineering Department, Ohio State University,
Columbus, OH 43210, USA

⁶Institut für Nichtlineare Dynamik, Universität Göttingen, D37073 Göttingen, Deutschland

⁷Max-Planck-Institut für Dynamik und Selbstorganisation (formerly Max-Planck-Institut für
Strömungsforschung), Bunsenstr. 10, D37073 Göttingen, Deutschland

(Received 31 October 2007 and in revised form 28 February 2009)

Since insight into entropy generation is a key to increasing efficiency and thereby reducing fuel consumption and/or waste and – for wall-bounded flows – most entropy is generated in the viscous layer, we examine the transient behaviour of its dominant contributor there for a non-canonical flow. New measurements in oil flow are presented for the effects of favourable streamwise mean pressure gradients on temporal entropy generation rates and, in the process, on key Reynolds-stress-producing events such as sweep front passage and on the deceleration/outflow phase of the overall bursting process. Two extremes have been considered: (1) a high pressure gradient, nearing ‘laminarization’, and (2), for comparison, a low pressure gradient corresponding to many earlier experiments. In both cases, the peak temporal entropy generation rate occurs shortly after passage of the ejection/sweep interface. Whether sweep and ejection rates appear to decrease or increase with the pressure gradient depends on the feature examined and the manner of sampling. When compared using wall coordinates for velocities, distances and time, the trends and magnitudes of the transient behaviours are mostly the same. The main effects of the higher pressure gradient are (*a*) changes in the time lag between detections – representing modification of the shape of the sweep front and the sweep angle with the wall, (*b*) modification of the magnitude of an instantaneous Reynolds shear stress with wall distance and (*c*) enlarging the sweeps and ejections. Results, new for both low and high pressure gradients, are the temporal behaviours of the dominant contribution to entropy generation; it is found to be much more sensitive to distance from the wall than to streamwise pressure gradient.

1. Introduction

For wall-bounded flows most entropy is generated in the viscous layer and knowledge of the entropy generation process is a key to reducing fuel consumption

† Email address for correspondence: dm6@inel.gov

and/or waste by increasing efficiency, so we study the transient behaviour of its dominant contributor there for a favourable streamwise gradient, a non-canonical flow warranting more research. Our approach is to extend the time series data of McEligot & Eckelmann (2006) to provide simultaneous ensemble-averaged distributions of this contribution in the vicinity of inclined shear layer (or sweep front) passage where it is maximal. In the process, new fundamental knowledge is obtained concerning the effects of pressure gradients on the turbulent structures known as sweeps and ejections and on their event rates.

As pointed out by McEligot and Eckelmann, laterally converging flow is one version of a group of flows which lead to favourable streamwise pressure gradients and, consequently, may modify characteristics of a turbulent flow. ‘Strong’ favourable pressure gradients have been found to reduce drag by altering the structure of the turbulent velocity fluctuations. In fact, with a favourable non-dimensional pressure gradient $K_p = (\nu/\rho u_\tau^3) dp/dx$ of the order of -0.03 an apparent ‘laminarization’ of a turbulent boundary layer (TBL) can occur (Narasimha & Sreenivasan 1979). (Here ν , ρ , u_τ , p and x denote kinematic viscosity, fluid density, friction velocity, static pressure and streamwise coordinate, respectively.) Related previous studies have been summarized by Narasimha & Sreenivasan (1979), Murphy, Chambers & McEligot (1983), Spalart (1986) and McEligot and Eckelmann (2006). As noted by Johansson, Alfredsson & Kim in 1991, little is known about turbulence in *non-canonical situations* such as significant pressure variation; this comment appears to be still valid.

This paper is the fourth in a sequence (Murphy *et al.* 1983; Chambers, Murphy & McEligot 1983; McEligot and Eckelmann 2006) delving successively deeper into the structure of laterally converging turbulent flows. The general question being addressed is – how is the turbulence structure in the viscous layer modified by the favourable streamwise mean pressure gradient induced by such a convergence? The experiment of McEligot and Eckelmann (2006) and the present study concentrate on the viscous layer (defined as the region where viscous effects are significant, but not necessarily dominant (Bradshaw 1975), typically taken to a distance from the wall $y^+ = yu_\tau/\nu$ of about 30 in a classical zero pressure gradient case – it includes the ‘laminar’ and ‘buffer’ sublayers in some investigators’s terminology). The superscript ‘+’ represents non-dimensionalization by ν and the friction velocity $u_\tau = (\tau_w/\rho)^{1/2}$ with τ_w symbolizing the mean wall shear stress. This viscous layer typically is the region where the largest gradients occur and the turbulence production is the largest. The major resistances to momentum, energy and mass transfer occur in this layer – and the pointwise entropy generation rate per unit volume S''' is greatest here as well. While some investigators consider that the effects of viscosity extend beyond ‘our’ viscous layer, say to $y^+ \approx 100$ or more (e.g. a kindly reviewer’s interpretation of the data of Morrison, Subramanian & Bradshaw 1992, p. 86 and McKeon *et al.* 2004), the direct or mean entropy generation rate decreases to about 1 % and the total dissipation rate to about 8 % of their wall values by $y^+ \approx 30$ (McEligot *et al.* 2008*b*).

Based on the results of McEligot & Eckelmann (2006) and the earlier studies cited by them, we can summarize the key observations concerning modifications of the *mean* turbulence structure in the viscous layer by favourable streamwise mean pressure gradients. There is evidence that the turbulence structure is modified. An effect of a favourable pressure gradient is to ‘thicken’ the viscous layer, in some senses; bursting rates are apparently reduced (Kline *et al.* 1967; Chambers *et al.* 1983; Finnicum & Hanratty 1988). The consequent upward shift in the logarithmic region as the Reynolds number is lowered was identified earlier via the mean velocity measurements of Senecal (1952); (McEligot, Ormand & Perkins 1966). Throughout

the remainder of this paper, the streamwise velocity is represented as $\tilde{u} = U + u$, where the tilde denotes an instantaneous quantity and upper- and lower-case letters symbolize the corresponding mean value and the fluctuation about it, respectively; the normal velocity \tilde{v} is treated in a similar fashion. Further details of the present experiment are provided in a report by McEligot, Brodkey & Eckelmann (2008c).

1.1. Background on entropy generation

Understanding of the behaviour of the entropy generation rate is important for several reasons. The local (pointwise) entropy generation rate per unit volume S''' is a key to improving many energy processes and applications (Bejan 1982). Bejan has suggested that real systems which owe their thermodynamic imperfections to fluid flow, heat transfer and mass transfer irreversibilities be optimized by minimizing their entropy generation. Since the loss of available work (Kestin 1980) is proportional to the amount of entropy produced (e.g. Btu/R or J/K), apparatus producing less entropy by irreversibilities destroys less available work, increasing the efficiency and, in turn, reducing fuel consumption and waste products. The pointwise S''' determines the localized contribution to energy losses or reduction in the availability of energy (Clausius 1887), so that insight into the dominant loss sources and their locations can allow reducing them intelligently, thereby improving efficiency.

Previous predictions of the *time-mean* behaviour in turbulent channel flows and boundary layers have shown that $(S''')^+$ increases as the wall is approached, that most entropy generation occurs in our viscous layer, that there is no significant dependence on Reynolds number in flows with negligible dp/dx and that there can be expected to be slight effects of favourable K_p (Rotta 1962; Bejan 1982; McEligot *et al.* 2008a, b). So we know in general where significant time-mean entropy generation occurs; in a sense, our *present interest* is to find *when* it occurs in terms of apparent coherent structures. Therefore we deduced measurements of temporal entropy generation which are *new for both l.p.g.* (low pressure gradient) and *h.p.g.* (high pressure gradient) conditions.

As shown by Bejan (1982) and others, the entropy generation rate per unit volume is given by $S''' = \mu\Phi/T$, where Φ is the dissipation function, μ is viscosity and T is the absolute temperature. The instantaneous dissipation function is given by Schlichting (1982, equation (12.8)) and others. In wall coordinates, one may evaluate the instantaneous entropy generation rate for incompressible flows as

$$S_t^+ = 2[(\partial\tilde{u}^+/\partial x^+)^2 + (\partial\tilde{v}^+/\partial y^+)^2 + (\partial\tilde{w}^+/\partial z^+)^2] + [(\partial\tilde{v}^+/\partial x^+) + (\partial\tilde{u}^+/\partial y^+)]^2 + [(\partial\tilde{w}^+/\partial y^+) + (\partial\tilde{v}^+/\partial z^+)]^2 + [(\partial\tilde{u}^+/\partial z^+) + (\partial\tilde{w}^+/\partial x^+)]^2$$

where S_t^+ is defined as $T\nu\tilde{S}'''/(\rho u_\tau^4)$ with the tilde, again denoting the instantaneous total value. Integration of this function with respect to time gives the familiar relations for dissipation of kinetic energy of the mean motion plus dissipation of turbulence kinetic energy ε , e.g. as by Rotta (1962, equation (7.1)) under boundary-layer approximations and by Gersten & Herwig (1992, equations (A1.21) and (A1.25)) for more general flows. These quantities are called ‘direct’ (or mean) and ‘indirect’ (or turbulent) dissipations, respectively, by authors studying entropy generation (Kock & Herwig 2004). In the present study, we aim to examine the transient behaviour of the instantaneous entropy generation (as defined above) and, therefore, the separation into ‘mean’ and ‘turbulent’ is not involved. In unheated flows with entropy generation solely due to friction as here, one can see that the instantaneous entropy generation rate is the same as the ‘instantaneous total dissipation rate’. However, thinking of entropy generation seems more appropriate for considering efficiency, lost work,

availability, etc. – and it extends directly to cases with additional irreversibilities, such as significant heat transfer (Kock & Herwig 2004).

Some further insight does come from studies concentrating on the time-mean dissipation of turbulent kinetic energy (t.k.e.). In boundary layers or comparable channel flows the term $(\partial U^+/\partial y^+)^2$ dominates the direct dissipation as noted by Rotta (1962). Likewise, Antonia, Kim & Browne (1991) indicate that in the viscous layer the term $(\partial u^+/\partial y^+)^2$ provides the dominant contribution to the indirect (turbulent) dissipation. Consequently, $S_{t,uy}^+ = (\partial \tilde{u}^+/\partial y^+)^2$ can be expected to be most important in evaluating S_t^+ . (The subscripts uy denote the partial differentiation of u with respect to y .) In studying the passage of internal turbulent shear layer structures, Johansson, Alfredsson & Eckelmann (1987) and Johansson *et al.* (1991) demonstrated that $\partial u/\partial y$ is greatest and considerably greater than $\partial u/\partial x$ there. Thus, it is $\partial u/\partial y$ that is expected to be a dominant contributor to temporal entropy generation. It will later be shown that the maxima of $\partial u/\partial y$ can be identified by detection of the maxima of $\partial u/\partial t$ in the time series data.

1.2. Models of coherent structures

Over the last several decades, many models have been hypothesized to explain the behaviour of fluid parcels in the important viscous layer and beyond (McEligot *et al.* 2008). These structures have been described variously. We continue to use the descriptions of Corino & Brodkey (1969). So called *sweeps* or *fronts*, which are events in a turbulent flow that displace the surrounding media due to their higher velocity, were first described by Corino & Brodkey (1969) from their visual studies and were further described by Nychas, Hershey & Brodkey (1973). An *ejection* is an abrupt movement outward from the wall area of fluid originally within this region. It occurred immediately after the start of an acceleration process and originated within the mass of fluid that constituted the prior retarded element. Often there was associated with these events a zone of high shear at the interface between the mean flow and the decelerated region that gave rise to the ejected element. Most ejections originated in the regions from y^+ about 5–15.

Wallace, Eckelmann & Brodkey (1972) ‘associated’ sweeps with events having positive u - and negative v -fluctuations (or ‘quadrant 4’ denoted by Q4) relative to the time-mean velocity in an Eulerian coordinate system. However, this definition does not exactly describe the essential characteristic of sweeps as being *fronts* of accelerated fluid. As known from the visual studies, these fronts are associated with large positive instantaneous gradients $\partial \tilde{u}/\partial t$ and with large positive spatial gradients $\partial \tilde{u}/\partial y$. Kreplin & Eckelmann (1979) observed that a steep front occurs in the near-wall region, out to y^+ about 50, with a convection velocity varying with wall distance. Due to the steep slope of this front, disturbances further from the wall are observed later at locations nearer the wall than away from the wall.

Several recent studies have proposed ideas, models, coherent structures and mechanisms to explain why wall turbulence is ‘self-sustaining’ (Robinson 1991; Panton 1997, 2001; Bernard & Wallace 2002; Adrian 2007). These studies typically have concentrated on fully developed pipe or ‘infinitely-wide’ channels or on zero pressure gradient boundary layers; consequently, effects of favourable pressure gradients have generally not been considered (even when significant as in low-Reynolds-number channel flows). A simple-minded view is that, in fully developed duct flows, wall turbulence is sustained by the continual pressure loss and, in boundary layers, by the continual transfer of momentum from the free stream. For the fully developed duct flow, the consequent skin friction coefficient is a function of a single parameter,

the Reynolds number, so all the various motions – that have been observed or hypothesized – must organize themselves so that this function is satisfied.

A potential benefit of detailed structure studies could be to identify their dominant aspects and how they would be modified by pressure gradients, property variation, compressibility or other phenomena and thereby be able to predict the effects of these phenomena. For example, the mean total shear stress profile, which the hypothesized motions must provide, may be approximated (Rotta 1962; Finnicum & Hanratty 1988) as

$$\tau^+\{y^+\} = (\tau\{y^+\}/\tau_w) = 1 + K_p y^+ - K_p y^+ (c_f/(2y^+)) \int_0^{y^+} (U^+)^2 dy^+$$

near the surface. The skin friction coefficient c_f here is defined as $2\tau_w/(\rho U_b^2)$ where U_b is a characteristic fluid velocity and the brackets $\{ \}$ indicate the functional dependence. For a flow with zero pressure gradient, $\tau^+\{y^+\}$ is inherently unity in the viscous layer while, for fully developed channel flow, the second term on the right-hand side becomes significant at low Reynolds numbers (as seen by the identity $-K_p = 1/Re_\tau$) and might be called a low-Reynolds-number effect. It would be desirable to examine the effects of lateral convergence (pressure gradient and streamwise acceleration) on the proposed models and various coherent structures – but only a few characteristics can be studied with simultaneous time series data from a single X-probe plus a wall sensor. In our present study, we employ the conditional sampling technique with averaging to deduce effects on $S_{t,uy}^+$ and – as a by-product – are able to identify some modifications of structure behaviour, primarily for sweeps or fronts and ejections.

1.3. Conditional sampling and averaging

Visual observations are the basis of descriptions of coherent structures. They have resulted in the dynamic pictures of coherent motions that we now call the ejections and sweeps (or fronts) of interest in the present experiment plus many others. Based on the observations, attempts have been made to extend the interpretations of the apparent motions to develop simple criteria to be able to classify the various events from examination of temporal measurements with thermal anemometry. As summarized by McEligot *et al.* (2008c), many techniques for conditional sampling and averaging of time series data in channel and boundary-layer flows have been developed and excellent reviews and/or analyses of these techniques are available. The reader is referred to this report and its citations for further details. However, it is appropriate to indicate key observations from the examinations of sampling that relate to or guide the present study.

Using Vita in a TBL, Blackwelder & Kaplan (1976) conditionally sampled $u\{t\}$ traces with detection based on identification of highly energetic fluctuations of u . Their conditionally averaged signal exhibited the same characteristics as the pattern recognition (PR) approach of Wallace, Brodkey & Eckelmann (1977): a weak deceleration followed by a strong acceleration. Wallace *et al.* (1977) concluded that the PR and Vita techniques detect the same aspect of the overall ‘bursting phenomenon’. As shown by Eckelmann & Wallace (1981), the *Vita detection* time $t^+ = (tu_\tau^2/\nu) = 0$ – when sampling $u\{t\}$ – corresponds to the maximum positive temporal slope in the conditionally averaged $\langle u^+ \rangle$ signal. (The brackets indicate an ensemble average.) They employed the data of Blackwelder and Kaplan to show that the maximum value of $(\partial \tilde{u}/\partial y)$ occurs at the same time as the maximum of $(\partial \tilde{u}/\partial t)$. Further, they demonstrated that, with the pattern recognition scheme of Wallace *et al.* (1977) $(\partial u/\partial y)_{max}$ also occurs when $(\partial u/\partial t)$ peaks. Therefore, either of these conditional

averaging schemes would be reasonable for examining the maximum temporal values of the entropy generation rate.

Ultimately, conclusions from conditional sampling will be *qualitative* for many aspects. Different investigators define the same structures variously and use conditional sampling techniques differently, so it is important to specify the present definitions and usage. If employed intelligently, one can use conditional sampling and averaging to deduce some characteristics of inclined shear layers (as with sweeps) and ejections. While Vita and PR detect fronts as in the sweeps described by Corino and Brodkey (1969), the quadrant-splitting (QS) approach can be a good method to detect ejections. As the threshold of QS is raised with Q2 detection, the identified structures approach the abrupt ejections of Corino and Brodkey rather than the minor outward flows of some dye trace visualizations. Measured event rates can be rather strong functions of the threshold levels, but the deduced flow patterns are much less dependent on threshold. Though these deduced flow patterns may be somewhat *qualitative*, relative timing between the events observed near detection can be considered to be *quantitative*.

1.4. *Conspectus*

The mean turbulence structure of the viscous layer with favourable pressure gradients is reasonably well understood now. The present objectives then are to determine whether streamwise mean pressure gradients affect the temporal behaviour of entropy generation rates in the viscous layer and, if so, which aspects are affected significantly. The experiment and analysis procedures are next presented briefly. The method of determination is by analysis of the time series measurements of McEligot and Eckelmann (2006). These data provide means to deduce the transient variation of the dominant contribution $S_{r,uv}^+$ and, in the process, yield information on effects of pressure gradient on structure event rates and ensemble-averaged $\langle u^+\{t^+\} \rangle$, $\langle v^+\{t^+\} \rangle$ and $\langle uv\{t^+\} \rangle^+$. Our observations are examined for pressure gradient effects on (a) structure event rates, (b) ejections via quadrant splitting and then, in the vicinity of the sweeps, (c) ensemble-averaged measurements of u^+ , v^+ , $(uv)^+$ and τ_w^+ and of (d) the dominant contribution to the instantaneous entropy generation rate. We summarize with a few concluding remarks. As with the measurements of Morrison & Westbury (1996), the insights afforded by the present results may also have significance to (a) the active control of wall turbulence and (b) development of wall boundary conditions in large eddy simulations (LES).

2. Experiment and analysis procedures

The equipment, procedures, experimental uncertainties and time series measurements employed in the present investigation are the same as those presented by McEligot & Eckelmann (2006). The data were obtained with X-probes and a wall-surface-probe using hot film sensors in the oil channel at the Max Planck Institut für Strömungsforschung. The channel was 22 cm wide and 1 m deep with a length of 8 m. Measurements examined two general situations: (a) a favourable streamwise mean pressure gradient induced via the lateral convergence of a 2° ramp installed on the floor of the channel and (b) for comparison purposes, approximately fully developed flow as in the earlier studies of Eckelmann and colleagues. Further understanding and specific details concerning the experiment are provided in the papers of Eckelmann (1974) and McEligot & Eckelmann (2006) plus a technical report by McEligot & Eckelmann (2003).

Only one X-probe was used at the measuring station in order to avoid the mutual interference between signals that can occur when employing a ‘rake’ of multiple sensors. However, since the time series for each run included the wall signal simultaneously with the signals from the two sensors of the X-probe, it is possible to relate the signals at the various wall-normal locations (y^+) via conditional sampling. Thus, one may form simultaneous ensemble averages for a range of y^+ without having additional probes to disturb the flow, i.e. one can construct the equivalent of two-component signals from a rake as by Blackwelder & Kaplan (1976) without actually having a rake of X-probes. This approach is comparable to that of Johansson *et al.* (1987) in examining the spatial distributions around an inclined shear layer in an l.p.g. channel flow. For the h.p.g. measurements at $y^+ \approx 16$, the estimated experimental uncertainty of $\langle \partial \tilde{u}^+ / \partial y^+ \rangle$ is of the order of 0.01 and for the resulting $\langle S_{t,uy}^+ \rangle$ is about 0.009, both in non-dimensional wall units. (It does not make sense to present per cent uncertainties because $\langle \partial \tilde{u} / \partial y \rangle$ in the denominator can pass through zero.) For the l.p.g. data at $y^+ \approx 13$, these uncertainties are of the order of 0.013 and 0.012, respectively.

Initially, three conditional-sampling techniques were used to examine the temporal behaviour of key coherent structures: (a) for ejections, the QS approach of Wallace *et al.* (1972) and Lu & Willmarth (1973) and, for sweeps, (b) the Vita analysis of Blackwelder & Kaplan (1976) and (c) pattern recognition as by Wallace *et al.* (1977). Each has advantages so different techniques can be applied for different purposes in examining temporal features of turbulence structure. Calculations are accomplished via a Fortran program developed by Wallace *et al.* (1977) as extended by Brodkey *et al.* (1985) and then modified slightly for the present work (to accommodate different sensor calibration approaches and to replace a five-sensor probe with an X-probe, the wall sensor and an upstream reference probe).

Johansson *et al.* (1987) used the Vita technique and simultaneous measurements from two sensors to construct the temporal and, hence, spatial fields in the vicinity of internal shear layer passage. Their constructed spatial field shows maximum values of $\partial u / \partial x$ and $\partial u / \partial y$ at detection (passage). By applying their Vita technique, which detects the passage of inclined internal shear layer structures, Johansson *et al.* (1991) were able to construct comparable spatial and temporal behaviour of $\langle u \rangle$, $\langle v \rangle$, $\langle uv \rangle$, $\langle p \rangle$ and turbulence production in the vicinity of this event from DNS of channel flow with a slight to moderate streamwise pressure gradient. Their conditionally averaged spatial fields in the x - y plane provide useful insight for interpreting the present Vita deductions for l.p.g. While Vita essentially triggers on high values of instantaneous $\partial u / \partial x$ (analogous to the $\partial u / \partial t$ of Vita), their figures 4 and 5 demonstrate that $\partial u / \partial y$ is considerably greater than $\partial u / \partial x$ there. *It is $\partial u / \partial y$ that is expected to be a dominant contributor to temporal entropy generation.*

For this paper a few defining comments on the analysis techniques are in order. One can consider detection as occurring when a signal exceeds a value given by a specified number times a ‘normalizing factor’. The Vita detection was applied to the time series for the streamwise fluctuation u . As by Blackwelder & Haritonidis (1983) the conditions for detection were that the variance defined by Blackwelder & Kaplan must exceed the quantity $k(u')^2$ (where u' represents the root-mean-squared value of the fluctuation u ; likewise for v) and the fluctuation must be increasing. The constant k served as threshold control and, by adjustment, determined the number of events detected. This detection corresponds to the timing of ‘fronts’ passing the probe location (Kreplin & Eckelmann 1979) or, in the interpretation of others, identifies

an ejection/sweep interface in the time series. As noted earlier, Vita detection is triggered by maximum values of du/dt which correspond to the desired maximum ($\partial \tilde{u}/\partial y$).

The QS technique aims at spotting the ejections described by Corino & Brodkey (1969) for their flow visualizations of pipe flow. Requirements for detection are that the peak value of the instantaneous $|-uv|$ exceed a quantity $HS \cdot u'v'$. If the wall normal fluctuation v is required to be away from the wall, it may be considered to be second quadrant detection (Q2) with its threshold controlled by the constant HS . In the process of examining the time series, all individual samples are categorized by their quadrants relative to the mean velocity and their 'instantaneous Reynolds shear stress' or turbulent momentum transfer rate is determined. Brodkey, Wallace & Eckelmann (1974*b*) were careful to point out that there does not exist a one-to-one correspondence between the visually observed motions and the quadrant categorizations. A Q2 event corresponds to a decelerating outward motion and a Q4 event to an accelerating wallward motion but, as noted earlier, not necessarily to abrupt ejections (Corino & Brodkey 1969) or sweep fronts (Kreplin & Eckelmann 1979). By choosing a sufficiently high threshold, QS detections can be limited to the abrupt ejections of Corino and Brodkey.

The pattern recognition process of Wallace *et al.* (1977) and Brodkey *et al.* (1985) overcomes some difficulties of other conditional-sampling approaches and tends to detect sweep front passage. In contrast to QS and Vita techniques, PR determines a short-term temporal (floating) average, called TPAV, for each specific event identified. It aims at accounting for shape and size of the transient events via a criterion for a signal slope (versus time) comparison ratio and the requirement that the maximum fluctuation Δu_{peak} for the event exceed a specified quantity 'AFACT' (as in amplitude factor) times the difference ($\tilde{u}_{max} - \tilde{u}_{min}$) calculated for the entire time series. This amplitude criterion was added to the computer program subsequent to the original publication by Wallace *et al.* (1977) and, along with other modifications, is explained by Brodkey *et al.* (1985). Adjustment of the required slope ratio and the constant AFACT establish the threshold for the sampling. PR also has the advantage of normalization of events to elucidate wave or event forms with few events required.

With each technique, once the sampling criteria are satisfied at an instant, all time series may be ensemble averaged about this time. Thus, temporal-ensemble-averaged traces for the two velocity fluctuations and the wall shear stress are related to the time of detection.

3. Results

McEligot & Eckelmann (2006) provided mean turbulence statistics in the viscous layer at $y^+ \approx 5, 7, 10, 15$ and 25 (nominal values) for four sets of operating conditions, two with favourable streamwise pressure gradients and two for the corresponding fully developed flows. As noted, the present objectives are to determine whether streamwise mean pressure gradients affect the temporal behaviour of entropy generation rates in the viscous layer and, if so, which aspects are affected significantly. In the present results we concentrate on the two extreme cases: $-K_p \approx 0.008$ for fully developed flow and $-K_p \approx 0.020$ (near laminarizing) for laterally converging flow. We conduct the conditional sampling for three wall distances $y^+ \approx 7, 15$ and 25 in order to represent temporal behaviour near the wall, in the region of greatest turbulence production and near the edge of the viscous layer, respectively.

3.1. Turbulent structure event rates

From different evidence Kline *et al.* (1967), Chambers *et al.* (1983) and Finnicum & Hanratty (1988) concluded that an effect of a favourable streamwise pressure gradient is to reduce an apparent bursting rate. These observations may be examined in terms of the various turbulent structures involved. One might expect that, with constant values of the threshold controls, the measured event rates may be compared across the viscous layer for the two extremes of pressure gradients. Since the detection techniques have different scaling factors (normalizing factors), the magnitudes should not be compared between techniques but their trends might be.

For these comparisons, the key parameters for the pattern recognition algorithm have been specified as AFACT = 0.4 with 'single point pinning' and a multiplier of 1.5 for the slope comparison ratio. For Visa, the averaging window has been adjusted to $(T_{avg})^+ \approx 10$ with $k = 0.32$ for the threshold. These two approaches are believed to detect sweeps. The QS subroutine can be programmed to detect apparent sweeps or ejections or both. The threshold HS for QS was 4.35 and the resulting data were further classified as Q2 or Q4; at this threshold they can be considered to represent the abrupt ejections and sweeps of Corino and Brodkey, respectively. Other secondary control parameters and constraints were also held fixed. The total sampling time was the same for all runs.

3.1.1. Reference condition – low pressure gradient

The trends of ejection and sweep rates for canonical flows are consistent with earlier observations which have been extensively reported in the literature. However, further physical explanations of this behaviour and apparent differences are in order.

Measurements of the numbers of sweeps and ejections detected are presented in figure 1(a) while non-dimensional event rates $f^+ (= f v / u_\tau^2$ where f is the number of events per unit time identified at a point) are provided in figure 1(b). Use of wall coordinates accounts for some variation with Reynolds number and perhaps pressure gradient. Here the data symbols are connected by solid lines for the h.p.g. case and by dashed ones for l.p.g. It would be logical that, very close to the wall, one would see a reduction in rate of ejections. But, over the rest of the layer, the induced ejection rate should be constant since they are part of the same event sequence no matter where they are deduced. In figures 1(a) and 1(b) only the pattern recognition events have the expected shape, i.e. their rates rise from a low value at the wall and become approximately constant away from the wall. For Vita and QS the turbulent structure rates vary with distance from the wall.

For the sweeps determined by both Vita and PR, one sees a tendency for the detection rate to increase with distance from the wall. However, the number of sweeps identified by the QS algorithm – based on the uv product rather than the streamwise fluctuation u – appears to decrease with distance from the wall; fewer exceed the $u'v'$ threshold. Since the thresholds are defined in physical variables here (rather than wall coordinates), the required magnitude variations to trigger sampling of the signals differ. For example for the l.p.g. run, the QS normalizing factor $u'v'$ is approximately equal to 0.46, 1.2 and 1.7 $\text{cm}^2 \text{s}^{-2}$, increasing successively, for the three locations examined ($y^+ \approx 5.6, 13.2$ and 22.2) while the corresponding values of the normalizing factor for Vita are $(u')^2 \approx 4.2, 9.2$ and 7.8 $\text{cm}^2 \text{s}^{-2}$, increasing then decreasing for the same locations. It could be interesting to define the sampling criteria in appropriate wall variables as suggested by Morrison, Tsai & Bradshaw (1989) but such a study is beyond the present scope.

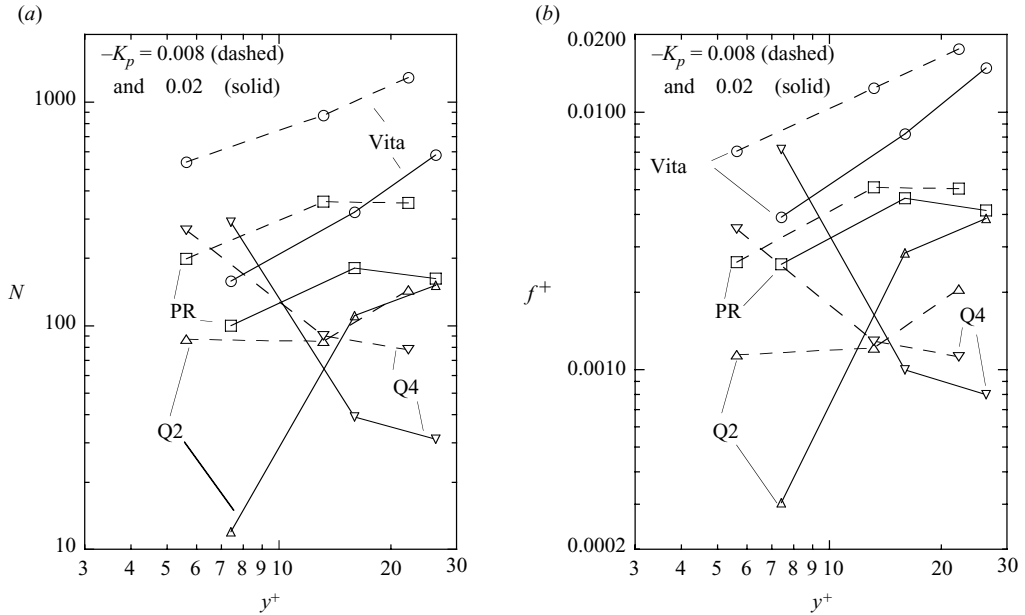


FIGURE 1. Sweeps and ejections identified across the viscous layer from conditional sampling by the Vita technique (sweeps, circles) (Blackwelder & Kaplan 1976), by pattern recognition, called PR (sweeps, squares) (Wallace *et al.* 1977) and by quadrant splitting (sweeps, triangles) (Wallace *et al.* 1972): (a) totals identified and (b) non-dimensional rates. Symbol Q2 represents ejections and Q4 sweeps; solid lines connect data at the higher streamwise pressure gradient ($-K_p \approx 0.02$) and dashed ones are for the lower pressure gradient ($-K_p \approx 0.008$).

The ejection rate from QS generally increases with distance from the wall. With the present level of the QS threshold criterion, significantly more ejections are detected than sweeps away from the wall while the reverse is true near the wall. Wallace *et al.* (1977) indicate that ejections originate somewhat further from the wall and move outwards while sweeps can and do come right up to the wall. The l.p.g. results for QS are consistent to some extent with earlier observations from several viewpoints: visual (Corino & Brodkey 1969), u , v and uv probability density functions (p.d.f.'s) (Brodkey *et al.* 1974b), pattern recognition (Wallace *et al.* 1977) and instantaneous 'production' (Eckelmann *et al.* 1977) – but these trends with y^+ are not obvious in the joint p.d.f.'s of Wallace & Brodkey (1977). Blackwelder & Haritonidis (1983) concluded that their bursting frequency f_b was a weak function of y but no region could be identified where f_b was independent of the Vita threshold. However, since the threshold multiplier was the same for all their data, the relative variation of frequencies reported cannot be attributed to it. They further concluded that the 'bursts' detected by Vita correlate well with large (uv) and f_b scales with wall variables.

With knowledge of some details of the detection technique and of typical time series across the viscous layer, one can provide a plausible explanation of the trend of sweeps identified by Vita versus y^+ . If the sweeps and ejections pass across most of the viscous layer as suggested by Corino and Brodkey, then for a given flow one would expect the detections/time to be approximately invariant with y . In this technique the threshold criterion is normalized by the local value of the mean square fluctuation; i.e. the calculated signal must exceed $k(u')^2$ to define a sweep. For our l.p.g. experiment $(u')^2 \approx 4.2, 9.2$ and $7.8 \text{ cm}^2 \text{ s}^{-2}$ for $y^+ \approx 5.6, 13.2$ and 22.3 , respectively. So in the outer

part of the viscous layer the required threshold level increases approaching the wall. Vita does not utilize u directly but rather a difference from a moving average – so it detects ‘rapid’ variations from the moving average, not the level of u . It is responsive to high values of the instantaneous $\partial u/\partial t$. The time series presented by Eckelmann (1970, figures 18–21) for $u\{t\}$ show that, as y^+ increases across the viscous layer, more small-scale rapid fluctuations appear in the signal. These fluctuations can introduce significant $\partial u/\partial t$ although only for brief intervals. So the rate of Vita sweep detections should increase with y (even if the threshold were not decreasing slightly).

In the QS technique the algorithm searches for instantaneous values of uv that are greater than the threshold criterion. From traces of $uv\{t\}$ (Eckelmann 1970, figure 28), one sees that the magnitudes and numbers of ‘significant excursions’ increase as y^+ varies from 3 to 20. So if one had a constant threshold, such as $HS \cdot u_t^2$, the detected numbers of QS events would likely increase with y^+ in the viscous layer. However, in the QS subroutine the threshold criterion is normalized by the product $u'v'$ so the instantaneous values of uv must exceed $HS \cdot (u'v')$ to identify sweeps or ejections. For our l.p.g. experiment ($u'v'$) \approx 0.46, 1.2 and 1.7 $\text{cm}^2 \text{s}^{-2}$ for $y^+ \approx$ 5.6, 13.2 and 22.3, respectively. The consequent variation of the threshold counters the trend of increased ‘excursions’ and, for example, the lower value of $u'v'$ near y^+ of five allows more events to be validated there. These identifications can be either ejections or sweeps, depending on the sign of v (in the present processing).

As noted, high values of the threshold multiplier HS , such as the current value 4.35, will limit the identifications to only the most ‘energetic’ events, corresponding to the abrupt ejections described by Corino and Brodkey (with the further requirement that $v > 0$). For qualitative insight into the question why more ejections may be detected towards the edge of the viscous layer one can consider a phenomenological description as in some explanations of Reynolds analogy (Kays 1966). For ejections outward from the low velocity region, if their x-momentum remains approximately constant, the magnitudes of their fluctuations $u = \tilde{u} - U$ will increase as they move towards the edge of the viscous layer where the local mean U is nearer to that of the ‘core’ or the free stream. Thus, the magnitude of the fluctuation uv becomes greater in the outer region of the viscous layer and it is more likely to exceed the QS threshold than when back in the environment where it originated. (Comparable ideas have been discussed in the context of transition as ‘lift-up effect’, low-speed streaks, ‘backward jets’, ‘blips’, negative ‘spikes’ and such (Liepmann 1943; Landahl 1980; Kendall 1998; Jacobs & Durbin 2001; Wundrow & Goldstein 2001). Equivalent reasoning will also qualitatively explain an increase in sweeps as the wall is approached. Consequently, the QS algorithm is more likely to detect sweeps near the wall and ejections towards the outer edge of the viscous layer.

3.1.2. *Effects of pressure gradient*

For both pressure gradients the trends with wall distance are essentially the same. When examined as numbers of events N detected at a point (figure 1a), the data representing sweeps generally show reductions as the pressure gradient is increased. In the outer part of the viscous layer the number of ejections detected is approximately the same for both pressure gradients. However, when the event rates are treated in terms of wall coordinates (f^+) the conclusions differ; some of the differences again can relate to the scaling of thresholds.

It is recognized that, between the techniques, the normalizing quantities vary differently with respect to pressure gradient and wall distance. Both $(u')^+$ and $(v')^+$ are functions of y^+ but, as predicted by Spalart (1986) and shown by McEligot

& Eckelmann (2006), $(v')^+$ is more sensitive to a favourable pressure gradient. Consequently, the normalizing quantity $u'v'$ in the threshold for quadrant splitting can be expected to change more with pressure gradient than $(u')^2$ and $(\tilde{u}_{max} - \tilde{u}_{min})$ in Vita and pattern recognition, respectively. (In later comparisons, thresholds have been adjusted for some runs to give approximately the same number of detected events across the viscous layer for ensemble averaging.)

If the wall behaviour for event rates at a point should scale with wall variables, as velocities, distances and time do without the effect of a pressure gradient, then one would expect that an appropriate basis for thresholds could be the same values in wall coordinates. For example, in sweep detection by Vita, using the same value of $k(u'^2)^+$ at the same location y^+ , would conceptually yield the same value of f^+ there. Since the present computer algorithm uses physical values of u' (cm s^{-1}), the same non-dimensional threshold would require setting $k_2 = k_1(u_{\tau 2}/u_{\tau 1})^2$ for the calculations at the second condition. If $u_{\tau 2} < u_{\tau 1}$ (as our h.p.g. is relative to the l.p.g. results), k_2 should be lower than k_1 . If k is held the same as is done in our comparisons, the threshold would be effectively higher in the second case – giving fewer detections N per unit time; but since N is not linearly related to u_{τ} , the conversion to f^+ may counter, but would not necessarily cancel, the effect of the higher effective threshold. The Vita and PR algorithms utilize the time series $u\{t\}$ for detection. McEligot & Eckelmann (2006) and others found $(u'\{y^+\})^+$ to be relatively insensitive to the pressure gradient, so this reasoning could apply. The observation that N decreased from l.p.g. to h.p.g. for sweep identification by these techniques is *consistent* with this idea. (Unfortunately, we no longer have the facilities to recalculate the results using the suggested value of $k_2 = k_{h.p.g.}$ so it does not prove it.) The QS algorithm is applied to the time series $uv\{t\}$ and we know that both $(v'\{y^+\})^+$ and $(\overline{uv}\{y^+\})^+$ are sensitive to pressure gradient (figures 4b and 5 by McEligot and Eckelmann). Hence, it is not clear what to expect of the QS technique as the pressure gradient is increased.

In terms of the non-dimensional event rates f^+ , the sweeps show reduced rates as the favourable pressure gradient is increased (with the exception of a possible anomaly for the point near the wall) as with N above. This observation is consistent with those of Kline *et al.* and Chambers *et al.* (1983). The apparent reductions in rates of sweeps are still seen but they are moderated by a reduction in u_{τ}^2 of over 40 % from the l.p.g. to h.p.g. case. However, as a consequence of this reduction in u_{τ}^2 , the non-dimensional ejection rate (from QS) then increases with pressure gradient in the outer part of the viscous layer. This result differs from the conclusions of Kline *et al.* (1967) and of Chambers *et al.* (1983). The latter experiment applied the Vita technique to the wall shear stress signal which Eckelmann (1974) has shown to behave as the streamwise fluctuation does; thus, Chambers *et al.* (1983) essentially detected the equivalent of sweeps. Kline *et al.* counted dye streak breakups F per unit time and per unit span and noted that interpretation of their numbers is not entirely clear. For example, the shape and trajectory of a dye parcel is a consequence of its historical path from injection; though looking like ejections, a breakup observed could represent fluid pushed ahead of a sweep – or some combination.

For the opposite situation of a strong adverse pressure, Krogstad & Skare (1995) found outside the viscous layer that the frequency of sweeps increases while the frequency of ejections decreases (using different non-dimensionalization for time than here). Aubertine & Eaton (2005) employed QS in the viscous layer (and across the boundary layer) to examine the effects of a mild adverse pressure gradient on the contributions to the Reynolds shear stress from the various quadrants but did not present effects on the related event rates.

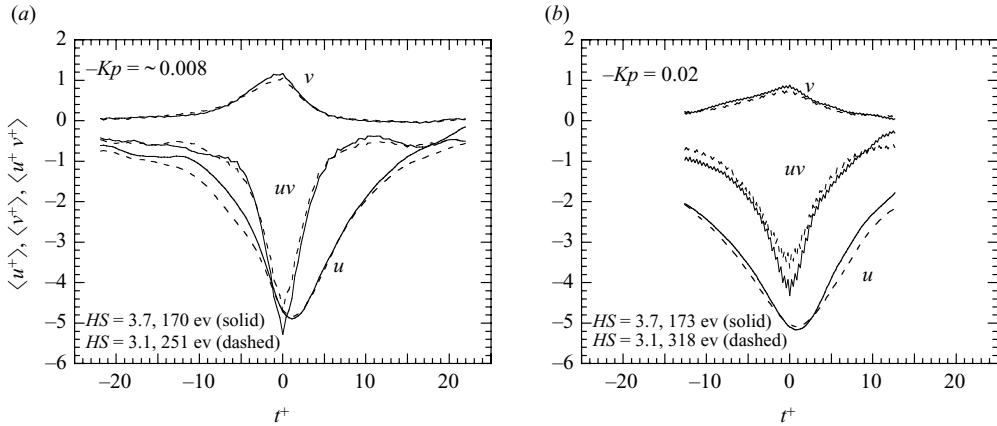


FIGURE 2. Transient behaviour of abrupt ejections identified by the QS technique: (a) lower pressure gradient ($-K_p \approx 0.008$, $y^+ \approx 13.2$) and (b) higher pressure gradient ($-K_p \approx 0.02$, $y^+ \approx 16$).

In summary, whether sweep and ejection rates appear to decrease or increase with the pressure gradient depend on the quantity examined and the manner of identification (and presentation). Authors need to be cautious in their generalizations of this topic.

3.2. Temporal behaviour of ejections

Some ensemble-averaged observations for the vicinity of the ejections identified by QS are shown in figure 2. These data are from the central region of the viscous layer at $y^+ \approx 13.2$ and 16.0 for l.p.g. and h.p.g., respectively. For these figures the algorithm was selected to identify ejections by requiring v to be away from the wall and uv to be negative. Time of detection ($t^+ = 0$) was taken as occurrence of a maximum value of $|-uv|$; consequently, the conditional average $\langle u^+v^+ \rangle$ peaks at $t^+ = 0$ by definition.

Two high levels of threshold multiplier HS were used to identify ‘abrupt’ ejections. One might ask the meaning of HS ; essentially it sets the level of ‘instantaneous Reynolds shear stress’ $|uv|$ required to trigger a valid detection in multiples of $(u'v')$. The higher the choice of HS , the more extreme are the events required to initiate sampling (i.e. further out on the ‘wings’ of the uv p.d.f.) and more likely to be tripped by one of the abrupt ejections observed visually by Corino & Brodkey (1969). One sees a slight effect on the peak value of $\langle u^+v^+ \rangle$ as higher thresholds lead to higher averages of the peak uv product being detected. However, the general effects on $\langle u^+ \rangle$ and $\langle v^+ \rangle$ behaviour (and $\langle u^+v^+ \rangle$ away from $t^+ = 0$) are slight in this range. Comparable behaviour was observed by Andreopoulos & Agui (1996) for ensemble averages based on detection of vorticity flux. For both l.p.g. and h.p.g., in this deceleration process the maximum outward fluctuation $\langle v^+ \rangle$ occurs in the range $-1 < t^+ < 0$ slightly before the observation of $\langle uv \rangle_{max}$ and it is followed by the minimum value of $\langle u^+ \rangle$ afterwards at t^+ near unity.

To examine the effects of the pressure gradient on these ensemble averages of temporal ejection behaviour, we concentrate on the results with a threshold multiplier of $HS = 3.7$ (solid curves) which gave about the same number of events in the two cases. The peaks are broader for the h.p.g. case, indicating that the deceleration process is slower in non-dimensional time (correlated over a larger range of t^+) or ejections

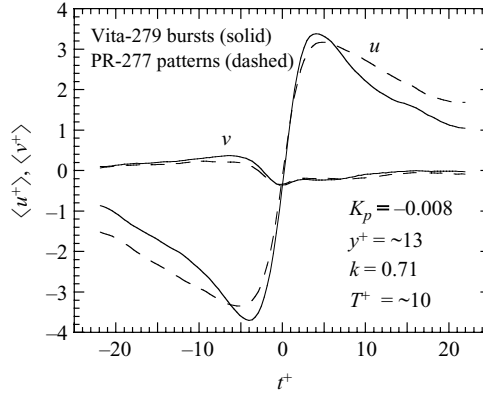


FIGURE 3. Comparison of transient behaviours of sweeps identified by pattern recognition technique (dashed curves) and Vita technique (solid curves) at $y^+ \approx 13.2$ in viscous layer of the lower pressure gradient experiment.

are larger in non-dimensional space. The minimum $\langle u^+ \rangle$ has approximately the same value for both. Thus, the difference in minimum $\langle u^+ v^+ \rangle$ is due to the magnitude of the outward component $\langle v^+ \rangle$. Although the threshold multiplier HS is the same for both l.p.g. and h.p.g., the peak values differ. On average, $-uv$ exceeded the threshold ($= 3.7u'v'$) by less for the h.p.g. case than the l.p.g. one, about 0.6 versus 1.6 in wall units. (This difference is consistent with the change in effective threshold when expressed in wall units.) The corresponding peak $\langle v^+ \rangle$ is reduced from about 1.15 to 0.85, indicating that the most 'energetic' ejections have smaller outward velocities for the higher pressure gradient. Since there is not a significant change of the peak $\langle u^+ \rangle$, these ejections have smaller angles with the outer flow. In the earlier paper, McEligot & Eckelmann (2006) likewise concluded from their probability density distributions that the vigour of ejections in the outer part of the viscous layer was less for the higher pressure gradient.

3.3. Temporal behaviour of sweeps as identified via pattern recognition

Since the pattern recognition and Vita approaches both identify sweeps giving the maximum value of $\partial u / \partial y$ (which is desired for calculation of the entropy generation), it is appropriate to compare their ensemble averages. Figure 3 demonstrates these averages at $y^+ \approx 13.2$ in our l.p.g. channel flow. Here single point pinning was selected for the PR subroutine rather than two-point time normalization and the PR time has been converted to t^+ for comparison. Control parameters were adjusted to detect approximately the same number of events with both techniques (AFACT = 0.4, filter width LFT = 25, slope comparison ratio = 1.5, ISIZE = 5, ITPAV = 10, $T_{avg}^+ \approx 10.2$ and $k = 0.71$). Slight differences are seen but effectively the same patterns and information are obtained.

The ensemble averages for Vita have slightly higher extreme values. For $t^+ < -4$, deceleration of $\langle u^+ \rangle$ is observed and $\langle v^+ \rangle$ is outward; an ejection is occurring. For PR the maximum outward velocity occurs at $t^+ \approx -9.9$ ahead of the minimum in $\langle u^+ \rangle$ at $t^+ \approx -5.1$ (with Vita detection the corresponding times are $t^+ \approx -6.6$ and -4.0). These portions of the averages correspond to those shown in figure 2 from ejection detection except the relative timing of peaks differs somewhat. The wall-normal fluctuation $\langle v^+ \rangle$ becomes inward at $t^+ \approx -2.9$ as the $\langle u^+ \rangle$ deceleration begins to abate. This section of the average from $t^+ \approx -2.9$ to about $+0.1$ corresponds

to a wallward interaction. Then the right side of the figure 3 beyond $t^+ \approx 0.1$ shows the characteristic behaviour of a sweep.

As also shown earlier by Wallace *et al.* (1977), Eckelmann & Wallace (1981) and others, figure 3 demonstrates that the observed temporal behaviour of sweeps is essentially the same whether identified by PR or Vita. Since the present study is interested in the simultaneous temporal behaviour (of $S_{t,uy}^+$) at different wall distances, we conduct our further examinations using the Vita technique since our implementation of it provides the desired ensemble averages directly as functions of t^+ .

3.4. Effects of pressure gradient on temporal behaviour of sweeps

A general overview of the sweep passage is presented as figure 4 for the two pressure gradients with each of the three probe locations. All results include 300 or more detected events. The X-probe and wall sensor provide four ensemble-averages: $\langle u \rangle^+$, $\langle v \rangle^+$, $\langle uv \rangle^+$ and $\langle \tau_w \rangle^+$. For the h.p.g. run, locations are $y^+ \approx 7.4, 16.0$ and 26.4 while they are $5.6, 13.2$ and 22.3 for the l.p.g. experiment. The wall shear stress trace is multiplied by a constant for visibility; otherwise the same scaling is applied to all subfigures for easy comparison. The timing of some of the key events is included in table 1. Due to the so-called ‘jitter’ (approximately random phase differences between key events) the amplitudes of the ensemble averages are moderated at large times $|t^+|$. Therefore, at large positive or negative times, the observations might be considered to be qualitative whereas near $t^+ = 0$ they are expected to be reasonably quantitative.

Since measurement of $\tau_w \{t\}$ is common to all probe locations and Eckelmann (1974) has shown that the instantaneous wall shear stress is similar to the instantaneous $u \{t\}$ fluctuation, the non-dimensional time t_w^+ is based on equivalent Vita identification at the wall sensor. As indicated by Eckelmann & Wallace (1981), the Vita detection with the u -signal typically occurs at the maximum positive gradient of $\langle \partial u / \partial t \rangle$; therefore, the equivalent detection time $t_w^+ = 0$ is defined as the time of the maximum positive gradient of $\langle \partial \tau_w / \partial t \rangle$. Thus, the traces for the three locations are placed on a simultaneous time basis as they would be if measured with a rake. These temporal distributions can be qualitatively considered to be ‘reverse images’ of the spatial distributions in the vicinity of the average sweep front (i.e. t^+ corresponds to $-x^+$).

The results from the h.p.g. experiment appear to be approximately the same as for the well-studied l.p.g. at corresponding locations. For both situations, the ensemble averages generally show first a Q2 deceleration continuing briefly ($\Delta t^+ \approx 2-4$) as a Q3 wallward interaction while the Q4 sweep interface approaches. Evidence of sweep front ‘arrival’ can be considered to be observation of an increase in $\langle u \rangle^+$ from its minimum and $\langle v \rangle^+$ becoming negative. Here interface passage then is defined as the time when $\langle u \rangle^+$ crosses zero. The ‘instantaneous Reynolds shear stress’ $\langle uv \rangle^+$ shows very little positive contribution in the vicinity of the front passage and none at the near-wall probe position. Near the wall the deceleration phase of $\langle u \rangle^+$ is slight while during acceleration it reaches values near 3. This observation is another indication that sweeps dominate the Reynolds stress near the wall; it is also evident in the $\langle uv \rangle^+$ variation which has its minimum in this phase. Also after front passage here $\langle -uv \rangle^+$ is much greater than the mean Reynolds shear stress. Away from the wall the deceleration is much greater, peaking at values near -4 while the acceleration does not exceed $\langle u \rangle^+ \approx 2$. The outward component $\langle v \rangle^+$ is likewise greater away from the wall during its ejection phase, corresponding to earlier observations that ejections dominate the Reynolds shear stress there (as demonstrated by the $\langle uv \rangle^+$ signature as well). In the central region of the viscous layer (subfigures 4*b* and 4*e*) the

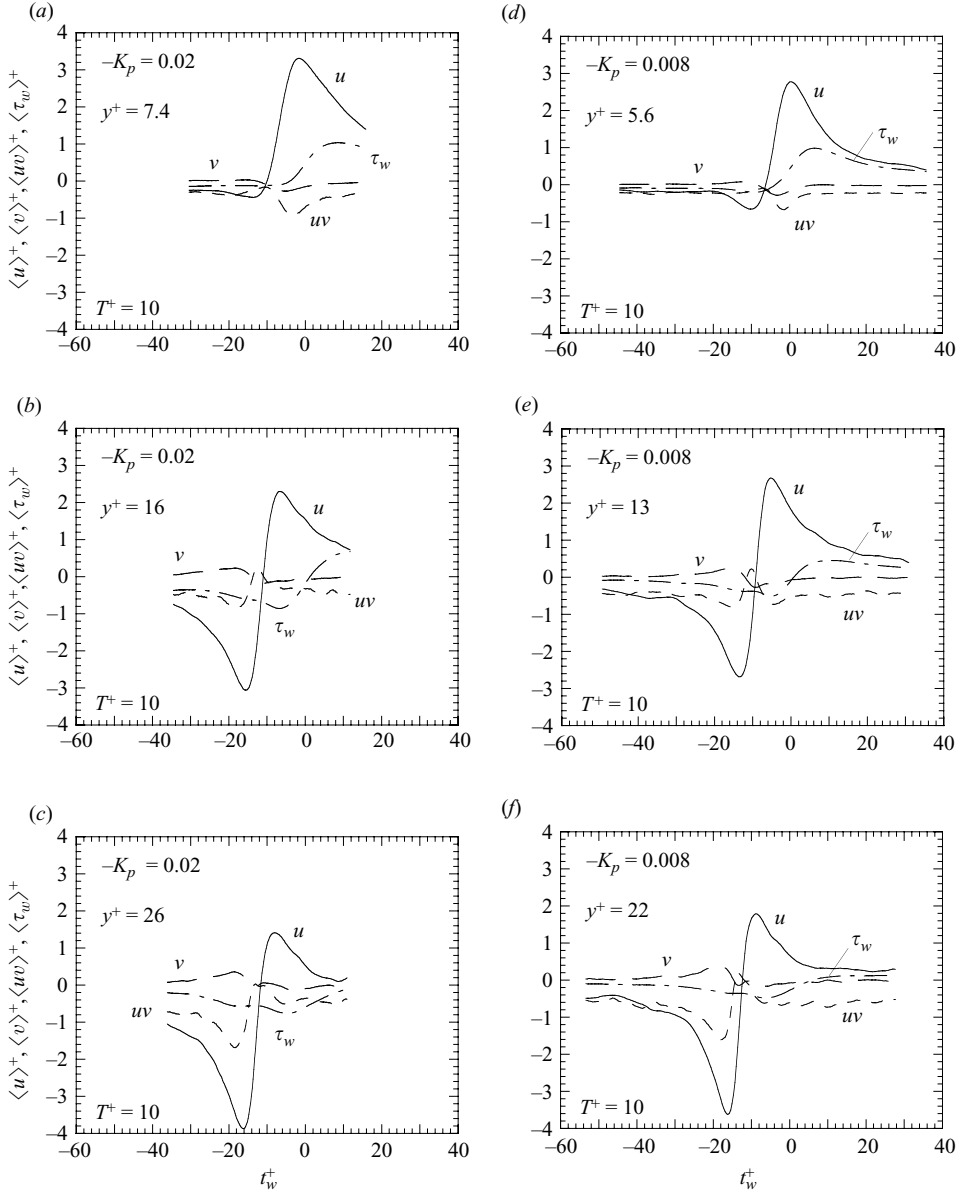


FIGURE 4. Transient behaviour of sweeps for h.p.g. (a)–(c) and l.p.g. (d)–(f) at three comparable locations across the viscous layer. The non-dimensional time $t_w^+ = 0$ is based on equivalent Vita detection for the $\tau_w\{t\}$ signal. (—, $\langle u \rangle^+$; — —, $\langle v \rangle^+$; - - -, $\langle uv \rangle^+$; · · ·, $\langle \tau_w \rangle^+$).

transient behaviours are intermediate in magnitude relative to those near and away from the wall; the $\langle u \rangle^+$ and $\langle v \rangle^+$ distributions are nearly antisymmetric, with the minima approaching the same magnitudes as the maxima. As the wall is approached the durations of the phases become broader corresponding to slower velocities.

While examination of transient turbulent production is not an aim of the present study, some basic comments may be made in passing. The following observations apply

$-K_p \approx 0.02$, h.p.g.	$y^+ \approx 7.4$	$y^+ \approx 16.0$	$y^+ \approx 26.4$
Max v^+ at t^+	+0.037 @ -15.5	+0.235 @ -18.0	+0.364 @ -18.8
Min uv^+ at t^+	-0.390 @ -19.5	-0.833 @ -17.9	-1.69 @ -18.4
Min S_{uy}^+ at t^+	0.368 @ -15.5	0.062 @ -16.2	0.0019 @ -21.4 and 0 @ -10.1, +1.5 and +7.7
Min u^+ at t^+	-0.435 @ -13.6	-3.05 @ -15.5	-3.87 @ -16.2
t_w^+ for $v^+ = 0$	-12.2	-14.2	-14.4, -12.2, -7.4 (oscillation)
Max uv^+ at t^+	-0.157 @ -10.7	+0.256 @ -12.5	+0.0344 @ -13.1
Min v^+ at t^+	-0.266 @ -5.0	-0.199 @ -11.8	-0.043 @ -13.1 and -0.115 @ -3.7
'Front' detection	-7.3	-11.4	-12.65
Max S_{uy}^+ at t^+	0.891 @ -4.8	0.275 @ -9.6	0.053 @ -12.5 and 0.023 @ -7.4
Max u^+ at t^+	+3.31 @ -1.8	+2.31 @ -6.6	+1.41 @ -8.1
Min uv^+ at t^+	-0.911 @ -3.5	-0.332 @ -5.5 and -0.483 @ +10.3 and 11.0	-0.505 @ -5.6 and -0.536 @ +8.1
$-K_p \approx 0.02$, h.p.g.	Interp. $y^+ \approx 5.6$	Interp. $y^+ \approx 13.2$	Interp. $y^+ \approx 22.3$
Min S_{uy}^+ at t^+	0.531 @ -15.5	0.0852 @ -15.8	0.0192 @ -18.1 and 0.0083 @ -6.3
Min u^+ at t^+	-0.252 @ -12.2	-2.38 @ -15.5	-3.85 @ -15.8
Max S_{uy}^+ at t^+	1.30 @ -1.8	0.475 @ -8.8	0.0914 @ -12.2
Max u^+ at t^+	+2.92 @ -1.5	+2.29 @ -6.3	+2.01 @ -7.4
$-K_p \approx 0.008$, l.p.g.	$y^+ \approx 5.6$	$y^+ \approx 13.2$	$y^+ \approx 22.3$
Max v^+ at t^+	+0.0814 @ -13.2	+0.249 @ -16.2	+0.385 @ -19.2
Min S_{uy}^+ at t^+	0.442 @ -13.3	0.0848 @ -16.2	0.00054 @ -17.7 and 0 @ -7.7 and -0.5
Min uv^+ at t^+	-0.241 @ -16.5	-0.801 @ -15.1	-1.60 @ -18.0
Min u^+ at t^+	-0.653 @ -10.3	-2.68 @ -13.3	-3.61 @ -16.2
t_w^+ for $v^+ = 0$	-8.4	-12.0	-14.7
Max uv^+ at t^+	-0.888 @ -7.0	+0.230 @ -10.4	+0.194 @ -13.6
Min v^+ at t^+	-0.279 @ -3.3	-0.267 @ -9.3	-0.141 @ -13.3 and -0.161 @ -6.3
'Front' detection	-4.42	-9.3	-12.89
Max S_{uy}^+ at t^+	1.149 @ -1.1	0.433 @ -7.7	0.640 @ -11.4 and 0.067 @ -5.5
Max u^+ at t^+	+2.78 @ +0.3	+2.67 @ -4.9	+1.79 @ -8.8
Min uv^+ at t^+	-0.671 @ -1.5	-0.729 @ -4.2	-0.622 @ -6.6 and -0.677 @ -2.2

TABLE 1. Non-dimensional times of occurrences of interesting events in the Vita signatures (all times in terms of t_w^+ ; $t_w^+ = 0$ at equivalent wall detection).

to both h.p.g. and l.p.g. cases. If one defines an 'instantaneous production' of t.k.e. as $\langle -uv \rangle^+ (\partial U^+ / \partial y^+)$ as by Diorio, Kelley & Wallace (2007), one sees that the time t_w^+ of its maximum varies with distance from the wall. (From their PR measurements, Eckelmann *et al.* (1977) showed that - at $y^+ \approx 30$ for an l.p.g. experiment - their instantaneous production was significantly greater than that defined by Diorio, Kelley and Wallace but their peak values occurred at approximately the same 'normalized time'.) Since $(\partial U^+ / \partial y^+)$ is independent of t^+ , one can examine the behaviour

of this version of ‘instantaneous production’ by observation of the signatures for ‘instantaneous Reynolds shear stress’, $\langle -uv \rangle^+$. Wilhelm, Härtel & Eckelmann (1998) found that an ‘instantaneous Reynolds shear stress’ ($-\rho uv$) generally showed high values and, therefore, intense production after interface passage. For the present data, near the wall the maximum $\langle -uv \rangle^+$ would likewise occur after the front passage. At this position figure 10(b) of Wilhelm *et al.* (1998) actually shows a slight maximum of $\langle -uv \rangle^+$ a bit ahead of their interface (with detection at $y^+ \approx 12.3$) but their front may be more curved than that of ours there. In the region of greatest mean production of t.k.e., i.e. in the central region of the viscous layer for l.p.g., local maxima of ‘instantaneous production’ would occur both before and after the frontal passage; for h.p.g. the same situation appears but the peak value is greater ahead of the front. In the outer part of the viscous layer, this maximum ‘instantaneous production’ would be predominantly earlier than the frontal passage, during the ejection phase. (However, Wilhelm *et al.* (1998) did not present any significant values of $\langle -uv \rangle^+$ in the ejection phase ahead of their front so comparison with the present data cannot be made there.)

The ensemble averages for both h.p.g. and l.p.g. are approximately the same at the same nominal locations y^+ . One may conclude that increasing the favourable pressure gradient does not cause large effects on the sweep behaviour. Chambers *et al.* (1983) had about the same comment concerning ensemble averages of $\tau_w \{t\}$ until K_v becomes large. However, there are differences in details.

In comparison to the l.p.g. experiment, near the wall for the higher pressure gradient there is a broader, higher peak in $\langle u \rangle^+$ with less deceleration in advance, $\langle v \rangle^+$ outward is less and $\langle -uv \rangle^+$ is greater in the sweep phase. Here there is greater lag between the u and τ_w detections. In the central region one sees a smaller contribution of $\langle -uv \rangle^+$ to Reynolds shear stress from inflow after the sweep passage for h.p.g. than for l.p.g. results (whereas ahead of the detection there, the outflow provides approximately the same peak values of $\langle -uv \rangle^+$ from both experiments). Further from the wall $\langle v \rangle^+$ is not as negative after the interface passage. So the sweep flow angle towards the wall is less there. And at these locations $\langle -uv \rangle^+$ is slightly less for h.p.g. in the sweep phase than for l.p.g. In the outer viscous layer the (non-dimensional) lag in detection is almost the same for both pressure gradients. In general, the ensemble averages for the h.p.g. experiment are broader or slower in non-dimensional time and longer in non-dimensional space than the l.p.g. results. The ‘peak-to-peak’ differences in $\langle v \{t^+\} \rangle^+$ are less for the h.p.g. case.

For both h.p.g. and l.p.g. conditions, one sees that the time interval between the u -detection and the τ_w -detection (i.e. their respective maximum gradients) increases with distance from the wall. This result corresponds to the observations of Kreplin & Eckelmann (1979) considering fronts. The fronts are pictured as being angled from the wall so the flow structure will intersect a probe away from the wall earlier than one near the wall. With DNS Wilhelm *et al.* (1998) showed further evidence that the fronts first discussed by Kreplin & Eckelmann (1979) are essentially identical to extended shear layers in near-wall flow. In good agreement with the experimental results, the front was found to be inclined to the wall from the linear layer into the logarithmic region. In the present results, there is an apparent change in the shape of the fronts as the pressure gradient is increased. To consider differences in front shapes, one can compare the non-dimensional lag from the u -detection to the τ_w -detection relative to y^+ for the two pressure gradients. Figure 5 provides this comparison as the difference $(t_w^+ - t_u^+)$ where t_u^+ is the non-dimensional time relative to the u -detection. For the l.p.g. experiment, the points near the wall are almost linear relative to the

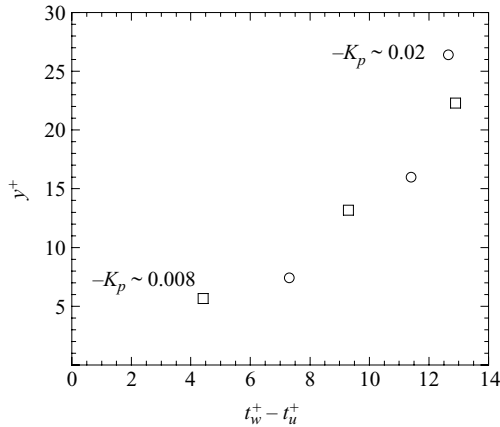


FIGURE 5. Front shape as indicated by non-dimensional time lag between u -detection and τ_w -detection (circles, $-K_p \approx 0.02$; squares, $-K_p \approx 0.008$).

origin and then there is greater curvature to the outer point. The h.p.g. front is more rounded than for l.p.g., appearing near parabolic and having a more acute slope near the wall. Propagation of the h.p.g. front in the near-wall region is slower – or one might interpret the figure as showing that there is quicker propagation in the outer region of the h.p.g. viscous layer giving a flatter form there.

Since the X-probe locations are not exactly the same in distance y^+ for the two pressure gradients, one may wonder whether some differences in detail are due to differences in non-dimensional position. Our conclusions above for front timing are valid since figure 5 is plotted in terms of actual non-dimensional probe locations. To compare the ensemble averages at equal distances, values of $\langle u \rangle^+$ for the h.p.g. experiment were interpolated to the same positions as in the l.p.g. measurements. Quadratic interpolation of $\langle u^+ \{ t_w^+ \} \rangle$ was applied to determine values of u^+ at the same non-dimensional instants t_w^+ at each of the locations y^+ . Then quadratic functions were fitted in the wall normal direction to deduce $\langle u^+ \{ y^+, t_w^+ \} \rangle$ at each instant at each probe location in the viscous layer. The results of the comparisons of shape and magnitudes at the same values of y^+ (not shown) for the two pressure gradients are essentially the same as the observations presented relative to figure 4. The lag between u - and τ_w -detections is consistent with figure 5. When compared at the same y^+ the interpolated values of $\langle u^+ \rangle$ for the h.p.g. conditions show slightly less deceleration ahead of the u -detection than at the actual probe locations further from the wall. The general trends observed for $\langle u^+ \rangle$ are still valid.

In summary, the main differences observable between the two pressure gradients during sweep passage are (a) changes in the time lag between detections – representing modification of the shape of the sweep front and the sweep angle with the wall, (b) modification of the magnitude of $\langle uv \rangle^+$ with wall distance and (c) broadening of the sweep fronts and ejections for the h.p.g. experiment.

3.5. Temporal behaviour of entropy generation rates and effects of pressure gradient

As the objective of the present work involves examining the transient entropy generation rates and since its maximum value occurs during the sweep, identification of the sweep and determination of the behaviour in its vicinity are needed. Application

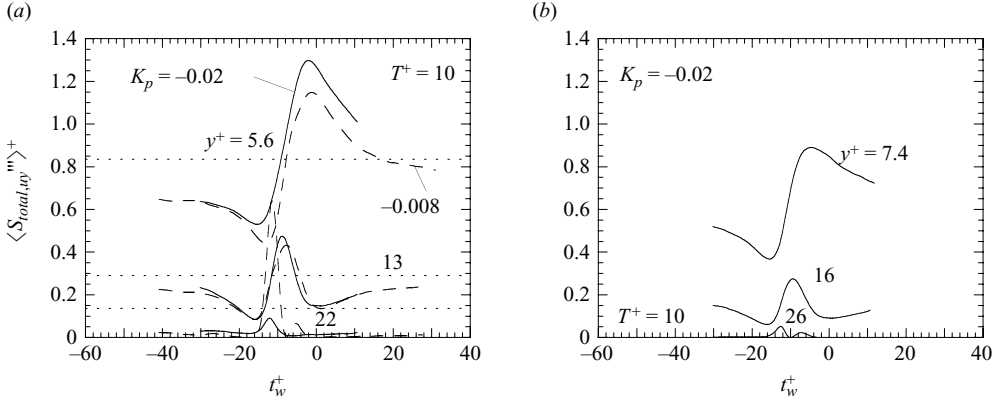


FIGURE 6. Transient behaviour of the dominant contribution to pointwise total entropy generation rate; h.p.g. case ($-K_p \approx 0.02$) identified with solid curves and low pressure gradient ($-K_p \approx 0.008$) with dashed curves: (a) at probe locations for l.p.g. experiment and (b) for h.p.g. experiment.

of the Vita technique to the time series $u\{t\}$ provides the means as it is known to detect maximum $\partial u/\partial t$ and, correspondingly, maximum $\partial u/\partial y$ (hence maximum $S_{t,uy}$).

Our ‘synchronized’ values of $\langle u^+\{t_w^+\} \rangle$ and $\langle v^+\{t_w^+\} \rangle$ allow calculation of a few terms contributing to $\langle S_t^+ \rangle$ including the dominant one. (Unfortunately, our data do not include spanwise measurements to deduce $(\partial \tilde{u}^+/\partial z^+)^2$ which is expected to be second in importance.) Quadratic interpolation of $\langle u^+\{t_w^+\} \rangle$ and $\langle v^+\{t_w^+\} \rangle$ was applied to determine values of these velocity components at the same non-dimensional instants t_w^+ in each of the experimental runs. After adding the mean values to obtain the instantaneous quantities at these instants, quadratic functions were fitted in the wall normal direction to deduce the dominant contribution $S_{t,uy}^+ = (\partial \tilde{u}^+/\partial y^+)^2$ at each probe location in the viscous layer. Thus, this process provides deduced synchronized ensemble-average results for $S_{t,uy}^+$ as functions of t_w^+ for each probe location in the viscous layer.

From figure 4 by Antonia *et al.* (1991) one can estimate values of the mean square gradients which could be deduced for evaluation of S^+ from X-probe data perpendicular to the wall. In the viscous layer, the time-mean values of $(\partial u^+/\partial x^+)^2$, $(\partial v^+/\partial y^+)^2$ and $(\partial v^+/\partial x^+)^2$ are predicted to be 0.0002–0.002, 0.001–0.003 and 0–0.001, respectively. These values are small compared to unity, the order of the direct dissipation $(\partial U^+/\partial y^+)^2$ near the wall. In the ensemble average $\langle u^+\{t_w^+\} \rangle$ the maximum value of $\partial u^+/\partial t^+$ is about 1.5 and occurs at the point of u -detection (the run at $Y^+ \approx 22.2$ and $-K_p \approx 0.008$ shows the steepest slope). With a conservative choice of $V_c^+ \approx 11$ for the convection velocity from Wilhelm *et al.* (1998), one may estimate the maximum ‘instantaneous’ value of $\langle \partial \tilde{u}^+/\partial x^+ \rangle^2$ to be about 0.02 – which is greater than the predicted mean value of $(S_t''')^+$ at this location but small relative to the desired peak values of $S_{t,uy}^+$. The estimated maximum values of $\langle \partial v^+/\partial y^+ \rangle^2$ and $\langle \partial v^+/\partial x^+ \rangle^2$ are found to be small in the same sense.

The new key results are provided in figures 6(a) and 6(b). To our knowledge, this temporal behaviour has not even been deduced for l.p.g. previously. Figure 6(a) provides $\langle S_{t,uy}^+ \rangle$ for the l.p.g. experiment as dashed lines and figure 6(b) shows this ensemble average for the h.p.g. one as solid curves. As before, the time $t_w^+ = 0$ is

equivalent to detection of interface passage based on the signal of the wall sensor which is common for each run. Also shown as horizontal dotted lines on figure 6(a) are the time-mean values of $\langle S_t \rangle^+$ for the l.p.g. experiment, including contributions from all spatial gradients (deduced from the DNS of Spalart 1988 for zero pressure gradient; McEligot *et al.* 2008b).

One sees that the general trends with y^+ and t_w^+ are the same in the l.p.g. experiment and the h.p.g. one but with some differences, particularly for the values nearer to the edge of the viscous layer. The levels of entropy generation rate decrease as y^+ increases; by the edge of the viscous layer (say $y^+ > 20$ or 30), $\langle S_{t,uy}^+ \rangle$ is small compared to the mean value of S_t^+ at the wall (predicted to be about 1.1–1.2). This transverse variation is consistent with DNS predictions of the time-mean entropy generation rate (McEligot *et al.* 2008a,b). Also the breadths of the peaks increase approaching the wall, indicating that the high temporal values of entropy generation rates last for longer durations near the wall. The main increase in $S_{t,uy}^+$ at a probe location y^+ appears near the front passage indicated by the earlier ensemble averages of $\langle u \rangle^+$.

The $\langle S_{t,uy}^+ \rangle$ results nearer the edge of the boundary layer show multiple peaks. Examination of these results with a logarithmic scale for the ordinate (not included) shows steep regions and very low values between the peaks, indicating that $\langle S_{t,uy}^+ \rangle$ may be approaching zero at these locations. From the tabulated values one can see that at some instants the velocity gradient $\partial \tilde{u}^+ / \partial y^+$ changes from positive to negative and vice versa. These observations are consistent with the measurements of Eckelmann & Randolph (1993, figure 1) using a gradient probe; they found that for y^+ greater than about 10, some individual samples of $\partial \tilde{u}^+ / \partial y^+$ were negative. This effect was not seen in our ensembles for y^+ of 16 and less where averages of more than 300 events were taken, thereby moderating effects of any extreme events. For the outer traces ($y^+ \approx 22.3$ and 26.4) the highest peaks come from positive values of $(\partial \tilde{u}^+ / \partial y^+)$ during sweep passage but they are followed by secondary peaks which correspond to negative gradients during the following deceleration phase.

Brodkey *et al.* (1974a) note that total dissipation (and therefore instantaneous total entropy generation rate) can be considered as a composite of local processes, one of which (observed visually) occurs in the high velocity gradient region that separates the decelerated flow (from which ejections originate) from the higher-speed sweep. If one interprets the detection as the instant of passage of an ejection/sweep interface, one can see that the peak of $\langle S_{t,uy}^+ \rangle$ generally is near the $\langle u^+ \{t_w^+\} \rangle$ maximum and, therefore, occurs slightly after the front passage. This delay is greater near the wall than for the measurements near the edge of the viscous layer. These observations are consistent with others for l.p.g. in showing that the maximum spatial gradient occurs near the front (Eckelmann & Wallace 1981; Randolph, Eckelmann & Nychas 1987). From their DNS and application of Visa sampling, Wilhelm *et al.* (1998) also essentially show that the highest values of $\langle S_{t,uy}^+ \rangle$ should occur shortly after the interface passage.

Further insight is obtained by comparing these figures to the related measurements of the fluctuations shown earlier in figure 4 (and to our tabulated results). Typical ensemble averages for these apparent events show a decrease in $\langle S_{t,uy}^+ \rangle$ corresponding to the deceleration in $\langle u^+ \rangle$ as t_w^+ increases, then a rapid increase with the front passage, followed by a gradual recovery to/towards previous levels. Though the temporal behaviour of $\langle S_{t,uy}^+ \rangle$ is deduced from the fluctuation $(u \{t_w^+, y^+\})^+$ and the mean velocity $U^+ \{y^+\}$, $\langle S_{t,uy}^+ \rangle$ is not an image of $\langle u \{t^+\} \rangle^+$. Near the wall the resemblance is close except that before sweep passage the reduction of $\langle S_{t,uy}^+ \rangle$ is greater than that

for $\langle u\{t^+\} \rangle^+$; this region is where sweeps dominate the Reynolds shear stress. Near the outer edge of the viscous layer, where ejections are more important for \overline{uv} than sweeps, the instantaneous positive and negative gradients of $\partial u^+/\partial y^+$ lead to multiple oscillations of $\langle S_{t,uy}^+ \rangle$ as opposed to the single oscillation of $\langle u\{t^+\} \rangle^+$.

The lowest entropy generation rate occurs during the Q2 deceleration phase and its maximum is slightly after interface passage. In §3.4 details of ensemble averages of the ‘instantaneous production’ of t.k.e. (which later generates entropy by dissipating), as defined by Diorio *et al.* 2007) have been treated. At the point near the wall this maximum production rate appears after sweep front passage, at about the same time as the maximum entropy generation rate. At the other two points further out, the largest production rate appears earlier than sweep interface passage while the maximum $\langle S_{t,uy}^+ \rangle$ still occurs during the sweep slightly after the interface passage.

Times of the occurrences of the maximum and minimum $\langle S_{t,uy}^+ \rangle$ and some other pertinent features are further documented in table 1. As the front approaches, first events are minimum $\langle S_{t,uy}^+ \rangle$, maximum $\langle v^+ \rangle$ and minimum $\langle uv \rangle^+$ with their apparent sequences differing with wall distance and sometimes with pressure gradient. In several cases the maximum outward $\langle v^+ \rangle$, presumably from ejections, appears at approximately the same time as the minimum $\langle S_{t,uy}^+ \rangle$; near the wall the minimum $\langle uv \rangle^+$ appears before these other two, during the gradual deceleration and outflow. Next comes the minimum $\langle u^+ \rangle$ or maximum deceleration, usually followed by the maximum $\langle uv \rangle^+$ or minimum ‘instantaneous Reynolds shear stress’ and then detection of the front. The minimum ‘instantaneous Reynolds shear stress’ – from the wallward interaction ahead of the front – occurs sequentially later as the wall is approached, corresponding to the slope of the front itself. Shortly after interface passage the maximum $\langle S_{t,uy}^+ \rangle$ occurs followed, in turn, by maximum $\langle u^+ \rangle$. The time interval between the first of these events (either the maximum outward $\langle v^+ \rangle$ or the maximum ‘instantaneous Reynolds shear stress’) and the final event, maximum $\langle u^+ \rangle$ from the sweep, is largest near the wall.

As would be expected from examination of $\langle u^+ \rangle$, one sees the same trends with respect to t^+ and y^+ at the two different pressure gradients but some differences are evident. Comparison of the deduced $\langle S_{t,uy}^+ \rangle$ results for $-K_p \approx 0.02$ (figure 6*b*) with those for $-K_p \approx 0.008$ (figure 6*a*, dashed curves) for comparable nominal probe positions could lead one to conclude that the effect of a strong pressure gradient is to reduce this temporal component of entropy generation, both its levels and its maxima. But this misleading conclusion is a consequence of the effective differences of the actual probe locations y^+ between the two experiments. Results have been calculated for the same runs as the earlier time series: $y^+ \approx 5.6, 13.2$ and 22.3 for $-K_p \approx 0.008$ (l.p.g.) and $y^+ \approx 7.4, 16.0$ and 26.4 for $-K_p \approx 0.02$ (h.p.g.). That is, the l.p.g. measurement locations are closer to the wall than the corresponding h.p.g. ones. Some differences between the two experiments may be explained by differences in y^+ relative to their nominal values. To account for this possibility, calculations for $\langle S_{t,uy}^+ \rangle$ in the h.p.g. experiment have been interpolated to the probe locations of the l.p.g. experiment as done earlier to check $\langle u^+ \rangle$. These interpolated values for h.p.g. are plotted as solid curves in figure 6(*a*). In contrast to the $\langle u^+ \rangle$ distributions, interpolation of $\langle S_{t,uy}^+ \{t_w^+\} \rangle$ for the h.p.g. cases to the same l.p.g. positions gives some significantly different observations.

While there are differences in detail in figure 6(*a*), particularly the maximum values, the trends are approximately the same for both $\langle S_{t,uy}^+ \{t_w^+\} \rangle$ at each common location. The maxima and minima occur at about the same times t_w^+ for both pressure gradients.

For the runs at $y^+ \approx 5.6$ and 13.2 the maxima and excursions from minimum to maximum are slightly greater for the h.p.g. experiment than the l.p.g. one. On average the h.p.g. value of $\langle S_{t,uy}^+ \{t_w^+\} \rangle$ has a higher level than for the l.p.g. at $y^+ \approx 5.6$ in contrast to the time-mean values of S_t^+ which are almost exactly the same at this location (McEligot *et al.* 2008a). That is, the sweep passage causes more entropy generation in its vicinity for the h.p.g. experiment. Away from the wall at $y^+ \approx 22$ the peak-to-peak oscillations of $\langle S_{t,uy}^+ \{t_w^+\} \rangle$ and its maximum value are much less for the h.p.g. case – but the average level is higher over this range of t_w^+ from deceleration to ejection to sweep to deceleration again for this case; at this location the DNS results of Spalart (1986) predict a slight reduction in the time-mean value of $(S_t)^+$ as the pressure gradient is increased. The first minimum value of $\langle S_{t,uy}^+ \{t_w^+\} \rangle$ occurs near the maximum ‘instantaneous Reynolds shear stress’ during the decelerating outflow phase ahead of the sweep; here the minimum $\langle S_{t,uy}^+ \{t_w^+\} \rangle$ is *not as low for the h.p.g.* experiment as for the l.p.g. except in the measurements in the central part of the viscous layer near $y^+ \approx 13$ where these values are approximately the same.

As seen in figure 4, the gradient $\langle \partial u^+ / \partial t^+ \rangle$ at interface passage is slightly greater at $y^+ \approx 22$ (l.p.g.) than for $y^+ \approx 26$ (h.p.g.), corresponding to a slightly higher gradient $\partial u^+ / \partial y^+$ and, therefore, higher $\langle S_{t,uy}^+ \rangle$ at that instant. The maximum value at $\Delta t^+ \approx 1.5$ later is also higher for this situation. While we concluded that $\langle u^+ \rangle$, $\langle v^+ \rangle$ and $\langle uv \rangle^+$ are generally broader in the h.p.g. experiment than in the l.p.g. one, one cannot make the same claim for the dominant entropy generation component (or the corresponding contribution to total dissipation). Though some coherent structures considered are apparently larger in wall coordinates, the timing of the transient variation of their entropy generation is not significantly affected.

In general, one may conclude that the dominant contribution $\langle S_{t,uy}^+ \rangle$ is much more sensitive to the distance from the wall than to an increase in favourable pressure gradient. The same qualitative observation can be made concerning the time-mean values of the direct and indirect (non-dimensional) entropy generation rates, as shown from DNS predictions for TBLs (McEligot *et al.* 2008b).

3.6. Implications for turbulence modelling

For wall-bounded turbulent shear flows, the primary aim of turbulence modelling would be prediction of the skin friction coefficient or the pressure drop with a secondary aim being to provide an adequate description of the velocity profile for prediction of thermal and species boundary layers. It was recognized in the 1960s that the so-called ‘Universal Velocity Profile’ and wall functions derived from it were not adequate for flows with significant pressure variation (Launder 1963; Patel 1965; McEligot *et al.* 1966). (For internal flows an empirical correlation was reasonable for c_f for $Re_D > 2500$ or $-K_p < 0.021$, Reynolds 1968.) This difficulty was cured with simple empirical modifications of mixing length treatments (McEligot *et al.* 1966; Huffman & Bradshaw 1972) and with early $k - \varepsilon$ models (Jones & Launder 1972).

The mean statistics of McEligot & Eckelmann (2006) and the present temporal observations can give some further insight. For more complicated turbulence models, the difficulties seen for scaling event rates as the pressure gradient increases imply that, in the important viscous layer, predictions will be sensitive to the choice of scaling or multipliers for their adjustable constants/functions. McEligot & Eckelmann (2006) data demonstrate that the Reynolds stress $\overline{u^2}$ does not vary significantly but $\overline{v^2}$ does in the outer region of the viscous layer. This observation may explain the success of the Durbin v^2-f model (Parneix, Durbin & Behnia 1998) for some complex flows, such as strongly heated gases with property variation (Hradisky *et al.* 2006). Beyond

the canonical flow assumptions of structure models (Panton 2001; Bernard & Wallace 2002) the various subgrid-scale models of large eddy simulations *may* (Xu *et al.* 2004) or may not (Hradisky *et al.* 2006) successfully predict complex cases.

In the present temporal observations, at $y^+ \approx 15$ for h.p.g. the ‘instantaneous Reynolds shear stress’ and the maximum outward velocities have smaller peak values during ejections but the sizes are larger than those for l.p.g. Timing of significant events relative to sweep passage implies larger coherent structures at the h.p.g. Timing and magnitude of the ‘instantaneous Reynolds shear stress’ and, therefore, ‘instantaneous production’ of t.k.e. per Diorio *et al.* (2007) are modified by the pressure gradient. To provide reasonable predictions for non-canonical flows, turbulence models should account for these effects of pressure gradients, either directly or indirectly. For some applications, the change in the shape of sweep fronts might be significant. These variations can be expected to have effects on the development of boundary conditions for LES (Morrison & Westbury 1996) and perhaps on other advanced turbulence modelling.

Morrison and Westbury interpreted their data as showing that small-scale turbulence is non-Gaussian and that this observation had consequences for LES where the subgrid-scale motion is often modelled by an eddy-viscosity hypothesis. Thus, use of an eddy viscosity in LES is likely to cause problems if used unquestioningly. As is well known, near the wall u and v are non-Gaussian with the probability density distributions of \tilde{v} and $(\tilde{u}\tilde{v})$ being affected by the pressure gradient (McEligot & Eckelmann, 2006). Consequently, subgrid-scale models must account for the pressure gradient somehow in this region; a sufficiently fine grid, approaching DNS, in the viscous layer may treat this difficulty. Turbulence modelling is beyond the scope of this paper so we invite sophisticated LES modellers to address this situation.

4. Concluding remarks

New fundamental measurements – for transient entropy generation rates and effects on coherent structures known as sweeps and ejections – have been obtained for turbulent flow in a converging duct, concentrating on the viscous layer where significant resistances to heat, momentum and mass transfer arise. A convergence induces a streamwise acceleration and, thereby, a favourable streamwise pressure gradient – a non-canonical situation. This paper is the fourth in a sequence delving successively deeper into the structure of these flows. The general question being addressed is – how is the turbulence structure in the viscous layer modified by the favourable streamwise pressure gradient induced by such a convergence?

This study extends the earlier work of Eckelmann and colleagues with the same facility. The present objectives then are to determine whether streamwise mean pressure gradients affect the temporal behaviour of entropy generation rates in the viscous layer and, if so, which aspects are affected significantly. Use of the oil channel permitted meaningful measurement of the wall-normal component and related statistics in the viscous layer where others could not obtain data due to problems of spatial resolution. Simultaneous time series data were obtained by McEligot & Eckelmann (2006) with an X-probe and a wall sensor to determine $\tilde{u}\{t\}$, $\tilde{v}\{t\}$ and $\tilde{\tau}_w\{t\}$. Measurements with the X-probe at $y^+ \approx 5, 7, 10, 15, 25$ (nominal values) and the centreplane concentrated on four sets of conditions of increasing severity of non-dimensional pressure gradient $-K_p$: two for fully developed flows and two for converging ones. Of these, the present study examines the two extremes: (a) a high pressure gradient, nearing ‘laminarization’, and (b), for comparison, a low

pressure gradient corresponding to many earlier experiments and direct numerical simulations. Temporal behaviours of the coherent structures were deduced via QS, PR and Vita techniques. Sufficiently high thresholds were employed so that sweeps and abrupt ejections were detected. The PR and Vita approaches gave about the same results so the latter was employed for most of the observations presented. The Vita approach with $\tilde{u}\{t\}$ is known to trigger on high values of $\partial u/\partial t$ corresponding to sweep passage and high values of the temporal entropy generation rate, so it is desirable to use it for the present objectives.

One might expect that, with constant values of the threshold multipliers, the measured turbulent structure rates might be compared across the viscous layer for the two extremes of pressure gradients. In terms of the non-dimensional event rates f^+ , the sweeps generally show reduced rates as the favourable pressure gradient is increased. This observation is consistent with those of Kline *et al.* (1967) and Chambers *et al.* (1983). In contrast, the ejection rate (from quadrant splitting) increases with pressure gradient in the outer part of the viscous layer. However, selection of threshold criteria on other bases could modify these results and, possibly, change the trends observed; we have discussed some of the related considerations and qualitative explanations of some earlier observations. Whether these rates appear to decrease or increase with the pressure gradient depends on the quantity examined and the manner of sampling (and presentation). Investigators need to be cautious in their generalizations of this topic.

Overall, the trends and magnitudes of the measurements are approximately the same for h.p.g. and l.p.g. when presented in terms of wall coordinates. For both situations, the ensemble averages generally show first a Q2 deceleration continuing briefly ($\Delta t^+ \approx 2-4$) as a Q3 wallward interaction while the Q4 sweep interface approaches. The main differences observable between the two pressure gradients for $\langle u^+ \rangle$, $\langle v^+ \rangle$ and $\langle uv \rangle^+$ are (a) changes in the time lag between detections – representing modification of the shape of the sweep front and the sweep angle with the wall, (b) modification of the magnitude of the ‘instantaneous Reynolds shear stress’ $\langle uv \rangle^+$ with wall distance and (c) broadening of the sweep fronts and ejections for the h.p.g. experiment.

Results new for even low pressure gradients are determinations of the temporal behaviour of the dominant contribution to entropy generation. The lowest entropy generation rate occurs during the Q2 deceleration phase and its maximum is slightly after interface passage. Typical sequences for the apparent bursting events, show a decrease in $\langle S_{t,uy}^+ \{t^+\} \rangle$ corresponding to the deceleration in $\langle u^+ \rangle$ as t_w^+ increases, then a rapid increase with sweep/front passage, followed by a gradual recovery to/towards previous levels. Also the breadths of the peaks increase approaching the wall, indicating that the high temporal values of entropy generation rates in the vicinity of sweep fronts last for longer durations near the wall. The main increase in $S_{t,uy}^+$ at a probe location y^+ begins at values of t_w^+ earlier than or ahead of the wall detection and near the front passage indicated by the earlier $\langle u \rangle^+$ results. For the runs at $y^+ \approx 5.6$ and 13.2 the maxima and excursions from minimum to maximum are slightly greater for the h.p.g. experiment than the l.p.g. one. Away from the wall at $y^+ \approx 22$ the peak-to-peak oscillations of $\langle S_{t,uy}^+ \{t_w^+\} \rangle$ and its maximum value are much less for the h.p.g. case – but the average level is higher over the range of t_w^+ from deceleration to ejection to sweep passage to deceleration again for this case.

One may conclude that the dominant contribution $\langle S_{t,uy}^+ \{t^+\} \rangle$ is much more sensitive to the distance from the wall than to an increase in favourable pressure gradient. The levels of entropy generation rate decrease as y^+ increases; by the edge of the viscous layer, $\langle S_{t,uy}^+ \rangle$ is small compared to the mean value of S_t^+ at the wall (predicted to

be about 1.1–1.2). The same qualitative observation on transverse variation can be made concerning the time-mean values of the direct and indirect (non-dimensional) entropy generation rates, as shown from DNS predictions for TBLs (McEligot *et al.* 2008*b*). For the most part, one can generally say that the level of pressure gradient within the range from slight to near laminarizing does not cause significant change in mechanisms but there are differences in detail relating to timing, sizes and shapes of sweeps and ejections – and therefore related details for some turbulence models.

The challenges remaining are now discussed. This paper has provided and summarized what might be called a ‘series of causes and effects’. It provides direct comparisons between l.p.g. and h.p.g. flows and at the same time offers more detailed observations and descriptions of the many results that we have obtained and some that are in the literature. It is a bit mind boggling as to how much has been observed over the nearly 40 years since the first papers began to appear on ‘coherent structures’. One might ask, ‘What has been accomplished in this period of time?’ Certainly, we know much more about the detailed interactions that occur in the flow, which are the causes and effects cited above. What then do we do next? What appears to be missing is an answer to the ‘why’? Can we generate a simple dynamic (instantaneous) cartoon of what is causing all of these phenomena? Can someone provide a video of an instantaneous flow as a function of time that can account for the myriad of details that are summarized here? Such a mechanistic picture could become the basis to model the flow for engineering purposes. Maybe then we could become more accurate in our projections and more cost effective in our designs.

We appreciate the kindly assistance of Professor James M. Wallace of U. Maryland, an architect of the original pattern recognition code, and Professor Ronald L. Panton of U. Texas who also provided advance copies of their recent journal manuscripts. The study reported was partly supported through the Long Term Research Initiative at the Idaho National Engineering Laboratory under DoE Idaho Operations Office Contract DE-AC07-76ID01570. Earlier incarnations were financed by the Applied Hydrodynamics Research Program of the Office of Naval Research (Dr James A. Fein, Program Manager), the National Science Foundation (Dr Win Aung, Program Manager), the U.S. Deutschland Fulbright Commission, the Max Planck Gesellschaft, the University of Arizona and Westinghouse Naval Systems Division (earlier Gould Ocean Systems Division). At the University of Limerick, Professor Mark R. D. Davies and Dr Edmond J. Walsh provided friendly encouragement and support enabling completion of this version of this paper. To all we are extremely grateful.

REFERENCES

- ADRIAN, R. J. 2007 Hairpin vortex organization in wall turbulence. *Phys. Fluids* **19**, 041301.
- ANDREOPOULOS, J. & AGUI, J. H. 1996 Wall-vorticity flux dynamics in a two-dimensional turbulent boundary layer. *J. Fluid Mech.* **309**, 45–84.
- ANTONIA, R. A., KIM, J. & BROWNE, L. W. B. 1991 Some characteristics of small-scale turbulence in a turbulent duct flow. *J. Fluid Mech.* **233**, 369–388.
- AUBERTINE, C. D. & EATON, J. K. 2005 Turbulence development in a non-equilibrium turbulent boundary layer with mild adverse pressure gradient. *J. Fluid Mech.* **532**, 345–364.
- BEJAN, A. 1982 *Entropy Generation Through Heat and Fluid Flow*. Wiley.
- BERNARD, P. S. & WALLACE, J. M. 2002 *Turbulent Flow. Analysis, Measurement and Prediction*. Wiley.
- BLACKWELDER, R. F. & HARITONIDIS, J. H. 1983 Scaling of the bursting frequency in turbulent boundary layers. *J. Fluid Mech.* **132**, 87–103.

- BLACKWELDER, R. F. & KAPLAN, R. E. 1976 On the wall structure of the turbulent boundary layer. *J. Fluid Mech.* **76**, 86–112.
- BRADSHAW, P. 1975 *An Introduction to Turbulence and its Measurement*, 2nd ed. Pergamon.
- BRODKEY, R. S., AOUAD, Y. G., VALIZADEH-ALAVI, H. & ECKELMANN, H. 1985 Refinement of pattern recognition of coherent structures in turbulent shear flows and a comparison between detection techniques. *Lec. Notes Phys.* **235**, 279–291.
- BRODKEY, R. S., TARABA, J. L., NYCHAS, S. G. & WALLACE, J. M. 1974a Reply to comments by P. Bradshaw. *Phys. Fluids* **17**, 2150.
- BRODKEY, R. S., WALLACE, J. M. & ECKELMANN, H. 1974b Some properties of truncated turbulence signals in bounded shear flows. *J. Fluid Mech.* **63**, 209–224.
- CHAMBERS, F. W., MURPHY, H. D. & MCELIGOT, D. M. 1983 Laterally converging flow. Part 2. Temporal wall shear stress. *J. Fluid Mech.* **127**, 403–428.
- CLAUSIUS, R. 1887 *Die mechanische Wärmetheorie*. Vieweg.
- CORINO, E. R. & BRODKEY, R. S. 1969 A visual observation of the wall region in turbulent flow. *J. Fluid Mech.* **37**, 1–30.
- DIORIO, J., KELLEY, D. H. & WALLACE, J. M. 2007 The spatial relationships between dissipation and production rates and vortical structures in turbulent boundary layers and mixing layers. *Phys. Fluids* **19** (3), 035101-1–035101-8.
- ECKELMANN, H. 1970 Experimentelle Untersuchungen in einer turbulenten Kanalströmung mit starken viskosen Wandschichten. Dissertation, Georg August Universität, Göttingen.
- ECKELMANN, H. 1974 The structure of the viscous sublayer and the adjacent wall region in a turbulent channel flow. *J. Fluid Mech.* **65**, 439–459.
- ECKELMANN, H., NYCHAS, S. G., BRODKEY, R. S. & WALLACE, J. M. 1977 Vorticity and turbulence production in pattern recognized turbulent flow structures. *Phys. Fluids Suppl.* **20**, S225–S231.
- ECKELMANN, H. & RANDOLPH, M. 1993 Measurements of spatial velocity gradients in a turbulent channel flow. In *Some New Trends on Fluid Mechanics and Theoretical Physics* (ed. C. C. Lin & N. Hu), pp. 358–361. Peking University Press (Conference was held in 1992).
- ECKELMANN, H. & WALLACE, J. M. 1981 A comparison of characteristic features of coherent turbulent structures found using the Variable Interval Time Average (VITA) technique and using the pattern recognition technique. *Lec. Notes Phys.* **136**, 292–303.
- FINNICUM, D. S. & HANRATTY, T. J. 1988 Effect of favourable pressure gradients on turbulent boundary layers. *AIChE J.* **34**, 529–540.
- GERSTEN, K. & HERWIG, H. 1992 *Strömungsmechanik*. Vieweg.
- HRADISKY, M., HAUSER, T., RICHARDS, A. & SPALL, R. 2006 Large eddy simulation of strongly heated internal gas flows. AIAA Paper, 2006-3260.
- HUFFMAN, G. D. & BRADSHAW, P. 1972 A note on von Kármán's constant in low Reynolds number turbulent flows. *J. Fluid Mech.* **53**, 45–60.
- JACOBS, R. G. & DURBIN, P. A. 2001 Simulations of bypass transition. *J. Fluid Mech.* **428**, 185–212.
- JOHANSSON, A. V., ALFREDSSON, P. H. & ECKELMANN, H. 1987 On the evolution of shear-layer structures in near-wall turbulence. *Advances in Turbulence* (ed. G. Comte-Bellot & J. Mathieu). Springer.
- JOHANSSON, A. V., ALFREDSSON, P. H. & KIM, J. 1991 Evolution and dynamics of shear-layer structures in near-wall turbulence. *J. Fluid Mech.* **224**, 579–599.
- JONES, W. P. & LAUNDER, B. E. 1972 The prediction of laminarization with a two-equation model of turbulence. *Intl J. Heat Mass Transfer* **15**, 301–314.
- KAYS, W. M. 1966 *Convective Heat and Mass Transfer*. McGraw-Hill.
- KENDALL, J. M. 1998 Experiments on boundary layer receptivity to free-stream turbulence. AIAA Paper 98-0530.
- KESTIN, J. 1980 Availability: the concept and associated terminology. *Energy Intl J.* **5**, 679–692.
- KLINE, S. J., REYNOLDS, W. C., SCHRAUB, F. A. & RUNDSTADLER, P. W. 1967 The structure of turbulent boundary layers. *J. Fluid Mech.* **30**, 741–773.
- KOCK, F. & HERWIG, H. 2004 Local entropy production in turbulent shear flows: a high-Reynolds number model with wall functions. *Intl J. Heat Mass Transfer* **47**, 2205–2215.
- KREPLIN, H.-P. & ECKELMANN, H. 1979 Propagation of perturbations in the viscous sublayer and adjacent wall region. *J. Fluid Mech.* **95**, 305–322.

- KROGSTAD, P.-A. & SKARE, P. E. 1995 Influence of a strong adverse pressure gradient on the turbulent structure in a boundary layer. *Phys. Fluids* **7**, 2014–2024.
- LANDAHL, M. T. 1980 A note on an algebraic instability of inviscid parallel shear flows. *J. Fluid Mech.* **98**, 243–251.
- LAUNDER, B. E. 1963 The turbulent boundary layer in a strongly negative pressure gradient. Master's thesis, MIT. Also MIT Gas Turbine Lab. Rpt. 71.
- LIEPMANN, H. W. 1943 Investigations on laminar boundary-layer stability and transition on curved boundaries. *NACA Wartime Report W-107*, ACR No. 3H30.
- LU, S. S. & WILLMARTH, W. W. 1973 Measurements of the structure of the Reynolds stress in a turbulent boundary layer. *J. Fluid Mech.* **60**, 481–511.
- MCELIGOT, D. M., BRODKEY, R. S. & ECKELMANN, H. 2008 Entropy generation in the viscous layers of laterally-converging duct flows. *Technical Report INL/EXT-08-14979*, Idaho National Laboratory, December. Available from the Information Bridge of the DoE Office of Scientific and Technical Information (www.osti.gov/bridge).
- MCELIGOT, D. M. & ECKELMANN, H. 2003 Effects of laterally converging flows on mean turbulence structure in the viscous layer. *Technical Report INEEL/EXT-2002-697*, Idaho National Engineering and Environmental Laboratory.
- MCELIGOT, D. M. & ECKELMANN, H. 2006 Laterally converging duct flows. Part 3. Mean turbulence structure in the viscous layer. *J. Fluid Mech.* **549**, 25–59.
- MCELIGOT, D. M., NOLAN, K. P., WALSH, E. J. & LAURIEN, E. 2008a Effects of pressure gradients on entropy generation in the viscous layers of turbulent wall flows. *Intl J. Heat Mass Transfer* **51**, 1104–1114.
- MCELIGOT, D. M., ORMAND, L. W. & PERKINS, H. C. 1966 Internal low Reynolds number turbulent and transitional gas flow with heat transfer. *J. Heat Transfer* **88**, 239–245.
- MCELIGOT, D. M., WALSH, E. J., LAURIEN, E. & SPALART, P. R. 2008b Entropy generation in the viscous parts of a turbulent boundary layer. *J. Fluids Engr* **130**, 061205-1–061205-12.
- MCKEON, B. J., LI, J., JIANG, W., MORRISON, J. F. & SMITS, A. J. 2004 Further observations on the mean velocity distribution in fully developed pipe flow. *J. Fluid Mech.* **501**, 135–147.
- MORRISON, J. F., SUBRAMANIAN, C. S. & BRADSHAW, P. 1992 Bursts and the law of the wall in turbulent boundary layers. *J. Fluid Mech.* **241**, 75–108.
- MORRISON, J. F., TSAI, H. M. & BRADSHAW, P. 1989 Conditional-sampling schemes for turbulent flow, based on the variable-interval time averaging (VITA) algorithm. *Exp. Fluids* **7**, 173–189.
- MORRISON, J. F. & WESTBURY, P. S. 1996 Perspectives on wall turbulence: the use of complementary techniques. *Exp. Thermal and Fluid Sci.* **13**, 211–222.
- MURPHY, H. D., CHAMBERS, F. W. & MCELIGOT, D. M. 1983 Laterally converging flow. Part 1. Mean flow. *J. Fluid Mech.* **127**, 379–401.
- NARASIMHA, R. & SREENIVASAN, K. R. 1979 Relaminarization of fluid flows. *Adv. Appl. Mech.* **19**, 221–309.
- NYCHAS, S. G., HERSHEY, H. C. & BRODKEY, R. S. 1973 A visual study of turbulent shear flow. *J. Fluid Mech.* **61**, 513–540.
- PANTON, R. L. (Ed.) 1997 *Self-Sustaining Mechanisms of Wall Turbulence*. Computational Mechanics Pubs.
- PANTON, R. L. 2001 Overview of the self-sustaining mechanisms of wall turbulence. *Prog. Aero. Sci.* **37**, 341–383.
- PARNEIX, S., DURBIN, P. & BEHNIA, M. 1998 Computation of three-dimensional turbulent boundary layers using the v^2 - f model. *Flow Turbul. Comb.* **10**, 19–46.
- PATEL, V. C. 1965 Calibration of the Preston tube and limitations on its use in pressure gradients. *J. Fluid Mech.* **23**, 185–208.
- RANDOLPH, M., ECKELMANN, H. & NYCHAS, S. G. 1987 Identification of sweeps with the help of the instantaneous velocity gradient dU/dy . *Advances in Turbulence*, pp. 408–415. Springer.
- REYNOLDS, H. C. 1968 Internal low Reynolds number turbulent heat transfer. PhD thesis, Aero. Mech. Engr., Univ. Arizona. Also DDC AD 669 254.
- ROBINSON, S. K. 1991 Coherent motions in the turbulent boundary layer. *Annu. Rev. Fluid Mech.* **23**, 601–639.
- ROTTA, J. C. 1962 Turbulent boundary layers in incompressible flow. *Progress in Aeronautical Sciences*, vol. 2, pp. 1–219, Pergamon Press.
- SCHLICHTING, H. 1982 *Grenzschicht-Theorie, Achte Auflage*. G. Braun.

- SENECAL, V. E. 1952 Fluid flow in the transition zone. PhD thesis, Carnegie Inst. Tech.
- SPALART, P. R. 1986 Numerical study of sink-flow boundary layers. *J. Fluid Mech.* **172**, 307–328.
- SPALART, P. R. 1988 Direct simulation of a turbulent boundary layer up to $Re_\theta = 1410$. *J. Fluid Mech.* **187**, 61–98.
- WALLACE, J. M. & BRODKEY, R. S. 1977 Reynolds stress and joint probability density distributions in the u - v plane of a turbulent channel flow. *Phys. Fluids* **20**, 351–355.
- WALLACE, J. M., BRODKEY, R. S. & ECKELMANN, H. 1977 Pattern-recognized structures in bounded turbulent shear flows. *J. Fluid Mech.* **83**, 673–693.
- WALLACE, J. M., ECKELMANN, H. & BRODKEY, R. S. 1972 The wall region in turbulent shear flows. *J. Fluid Mech.* **54**, 39–48.
- WILHELM, D., HÄRTEL, C. & ECKELMANN, H. 1998 On the relation between fronts and high-shear layers in wall turbulence. *Flow Turbul. Comb.* **60**, 87–103.
- WUNDROW, D. W. & GOLDSTEIN, M. E. 2001 Effect on a laminar boundary layer of small-scale streamwise vorticity in the upstream flow. *J. Fluid Mech.* **426**, 229–262.
- XU, X., LEE, J. S., PLETCHER, R. H., SHEHATA, A. M. & McELIGOT, D. M. 2004 Large eddy simulation of turbulent forced gas flows in vertical pipes with high heat transfer rates. *Intl J. Heat Mass Transfer* **47**, 4113–4123.